Universität Hamburg

Synchrotron Research Institute

YEREVAN STATE UNIVERSITY

German-Armenian Joint Practical Course
on Accelerator Physics

Vibrating wire monitors and beam profile measurements

Supervisor: Dr Suren G. Arutunian

PIER
Partnership of
Universitat Hamburg and DESY

YEREVAN, ARMENIA
2025

Contents

The scope of the work

The course includes a detailed overview of existing beam profiling methods: beam scintillator screens, secondary emission monitors, wire scanner, multi-wire proportional chambers, residual gas monitors, optical transition radiation monitors, synchrotron radiation monitors, laser wire scanner. The specific parameters and usage features of different technics are presented.

In the course students will be familiarized with a new diagnostic instrument for beam profile measurement – the Vibrating Wire Monitor (VWM), the operation principle of which is based on a simple and clear idea of a mechanical resonator (stretched wire) and its frequency dependence on the wire tension. The wire tension, in turn, depends on its temperature, i.e. the instrument is essentially a precise thermometer. The dependence of the wire temperature on its position in the beam determines the beam profile. A wide dynamic range (in the temperature equivalent to fractions of milli Kelvin to hundreds of degrees), high accuracy of the measurements, good long-term stability, resistance to high background radiation and electromagnetic interference, and digital nature of the measurement of the output value (i.e., the frequency of natural oscillations of the wires) make this method a versatile tool for measuring the profiles of beams of charged particles, electromagnetic radiation, and neutrons in a wide range of energies. The large dynamic range, in particular, allows for measurements in both the halo and core of the beam.

1. Beam profile measurement in accelerators

Measurement of beam profiles in accelerators is one of the important tasks of accelerator diagnostics. As in the other areas of diagnostics, a number of methods aimed at solving specific problems related to beam profile measurement are discussed. Especially, it is important to note a significant difference in diagnostics during the accelerator construction and commissioning process and diagnostics during accelerator operation. In the first case, as a rule, the task of steering the beam constitutes a certain stage in the acceleration process. The large number of bending, focusing and correction magnets give rise to the need for many profile measurements [1]. At this stage, methods that completely destroy the beam can be used.

In contrast, in the second case, it is required to apply methods of minimally influencing the beam and providing online information on the quality of the beam. For example, it is important to control the beam width, position and distribution in transversal directions. Another important parameter is the speed of the measurement, which is also determined by the tasks. Measuring the cross-sectional profile of an individual bunch and the average of a beam are very different tasks requiring completely different techniques. The type of accelerator also determines the difference in diagnostic methods. Therefore, the methods permissible in single-pass linear accelerators would destroy the beam in accelerator types with closed multiturn cycles. The current and energy of the particles are also essential parameters, which dictate the choice of certain measurement schemes. Accelerators with very high current dictate specific methods of diagnostics. For example, in the International Fusion Materials Irradiation Facility project (also known as IFMIF), which is aimed to fully qualify materials for fusion reactor, the current of the two 40 MeV deuterons beams reaches 125 mA. This makes difficult the

installation of certain measurement devices, and diagnostics can be made exclusively by contactless methods or only at the periphery of the beam[1].

In beam profiling, the level of requirements for profile detailing is important. In some cases, information on the distribution of particles only in the central region of the beam is sufficient. For the Gaussian particle distribution model, this corresponds to a 3-4 sigma (core) profiling. In other cases, it is necessary to provide a larger dynamic range, which allows measurement of the profile outside the central region in a so-called halo region. This problem is especially relevant for accelerators with a long beam lifetime, where particle losses occur through particle leaks through the halo region.

In this review, we present the main methods for measuring beam profiles in accelerators.

1.1. Beam profile

Transverse beam profiles express the particles distribution in a beam as a function of the transverse position, thus we have a horizontal profile expressing the number of particles at different horizontal positions, and we have a vertical profile expressing the number of particles at different vertical positions [2].

As a rule, the aim of the transversal beam profile measurement in the beam core is to determine the transverse shape of the beam up to about 3 to 4 sigma. Therefore, a dynamic range of 10^3 to 10^4 is sufficient for a single measurement [3].

All profile measurement methods can be divided into two classes: 1D and 2D [2].

In the one-dimensional sampling the following instruments are traditionally used:

- Wire scanners
- Wire grids
- Rest gas ionization monitors
- Laser wire scanners

In the two-dimensional sampling, techniques based on screens and radiators are usually used. In circular machines, synchrotron radiation is often applied as a 2D replica of the beam profile. Taking advantage of the rapid development and the huge market for commercially available optical sensors, in the past years optical measuring techniques took on a greater significance. Nowadays area scan CCD or CMOS sensors are widely used in beam diagnostics because they provide the full 2D information about the transverse particle beam distribution, allowing in principle to investigate shot-to-shot profile fluctuations at moderate repetition rates.

In general, there are two types of measurement methods: Nearly non-destructive devices and destructive devices [2, 4]:

- nearly non-destructive devices, such as harps, profile grids, SEM grids, residual gas ionization monitors, viewing screens (holds only if the penetration depth is large in comparison to the screen thickness), and wire scanners,

[1]IFMIF-EVEDA, IN-IF-ACXX-0xx, Beam Instrumentation Preliminary Design Review, June 2010, Beam Instrumentation, IFMIF PDR.pdf.

- destructive devices, such as segmented Faraday cups, Faraday cups combined with scanning slits, and sandwich detectors used for emittance measurements.

It should be stressed that there is an important difference between beam tails and beam haloes: tails are deviants from the expected beam profile in the order of percent or per mille while haloes are much smaller in intensity. Fig. 1 shows two examples of beam tails and beam halo to visualize this difference. Since profile measurements are often questioned at the level of a few percent, e.g., by instrumental uncertainties, the difficulty is easily seen in making halo measurements already at the level of 10^{-4} and beyond [4, 5]

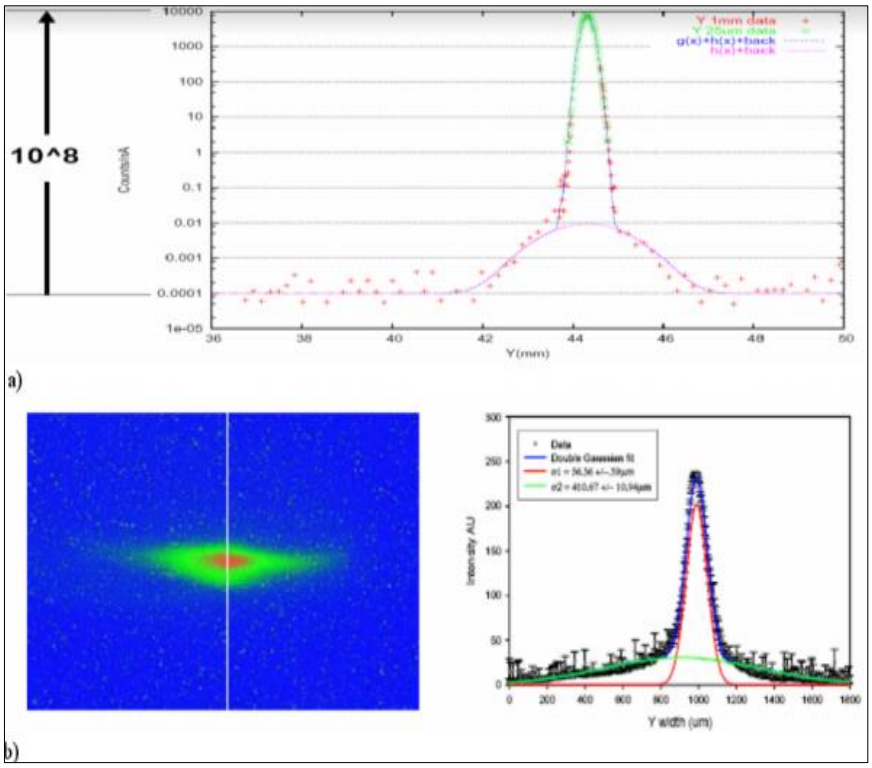

Fig. 1. (a) Beam halo determination with a dynamic range of 10^8; (b) The green curve is a halo and not a tail (which is the low amplitude part of the red curve) [5]. Note the logarithmic vertical scale in both diagrams.

1.2. Beam Scintillator Screens

The most direct way of beam observation is the light emitted from a scintillation screen, monitored by a commercial video or CCD camera, see e.g. [1] for an overview (see also[2],[3]). A scintillator screen (often called phosphorescent, fluorescent or luminescent) is moved into the path of the beam [6]. Scintillators were the first particle detectors, more than a century ago. When accelerators, instead of cosmic radiation and radioactive samples, began to deliver particles, scintillators were the prime means to detect the existence of a beam and its location. In contrast to OTR (see below), the scintillation light is emitted isotropically, i.e. there is no restriction on the observation geometry and both the screen and the camera can be placed under arbitrary angles with respect to each other [7].

[2] R. Jung, G. Ferioli, S. Hutchins, SINGLE PASS OPTICAL PROFILE MONITORING, Proc. Diag. Instrum. Part. Acc. Conf., DIPAC03, Mainz, 2003, p. 10-14.
[3] P. Forck, C.A. Andre, F. Becker, R. Haseitl, A. Reiter, B. Walasek-Höhne, W. Ensinger, K. Renuka, Scintillation Screen Investigations for High Energy Heavy Ion Beams at GSI, Proc. Diag. Instrum. Part. Acc. Conf. DIPAC11, Hamburg, 2011, pp. 170-173.

These devices are installed in nearly all accelerators from the source up to the target and are schematically shown in Fig. 2 together with a realization where the pneumatic feed-through is mounted on a Ø200 mm flange.

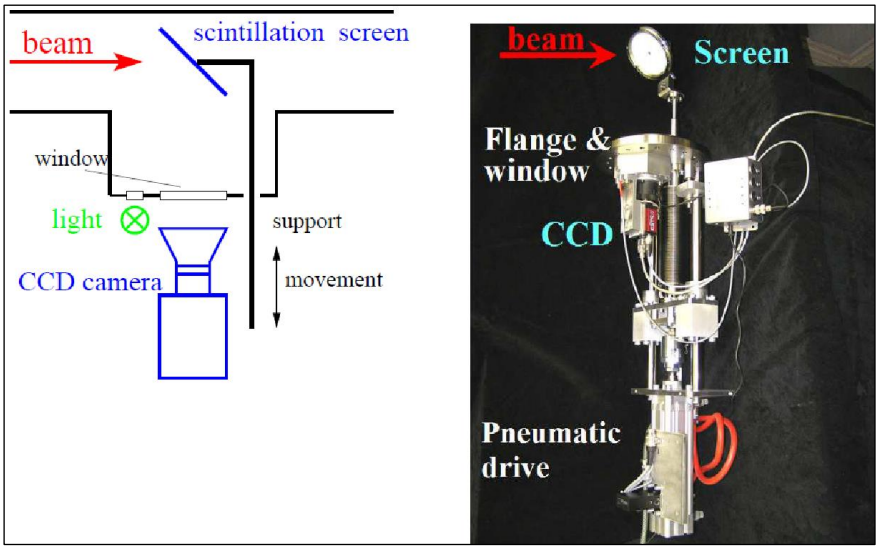

Fig. 2. Layout of an intercepting scintillator screen is shown on the left side. On the right side there is a photo from a P43 phosphor scintillation screen of Ø70 mm and the CCD camera are mounted on a Ø200 mm flange with pneumatic feed-through [1].

The most common scintillator is used to be ZnS powder which, with some binder, was painted onto a metal plate. Such screens deliver green light and have high efficiency but are unfit to use in high vacuum and are burnt out at some 10^{14} protons/cm^2 at GeV energies. A great step forward was the formation of thick Al_20_3 layers on aluminum plates under simultaneous doping with Cr. Chemically, this is the same as ruby and the light emitted is red. These screens are fit for ultra-high vacuum and have a long lifetime (10^{20} to 10^{21} protons/cm^2 at 50 MeV) [6] (see Fig 3, Fig4).

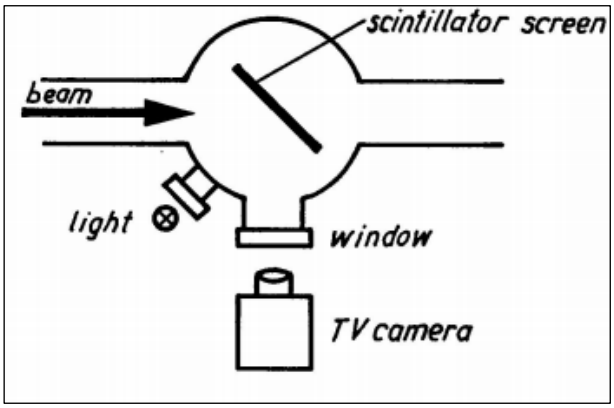

Fig.3. Typical arrangement for observation of the beam position and size with a movable scintillator screen and a TV camera [6].

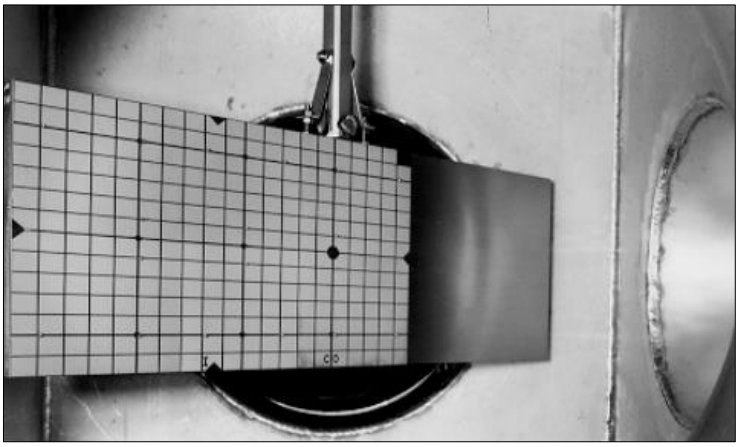

Fig. 4. Scintillator screen made from a Cr-doped Al_2O_3 plate with imprinted graticule [6].

Crystal scintillation screens are also frequently used as scintillation materials. Standard scintillation materials used for imaging screens include YAG:Ce, LuAG:Ce (ideal for consecutive photodiode and avalanche photodiode readout), and YAP:Ce (suitable for readout in the ultraviolet range)[4].

When a charged particle penetrates a material, the energy loss can be transformed to fluorescence light. The important properties of such a scintillator are [1]:

- High light output matched to the optical system of the CCD camera in the optical wavelength range (450 nm < λ < 700 nm).
- High dynamic range, i.e., a good linearity between the incident particle flux and the light output. In particular, a possible saturation of the light gives rise to a deformation of the recorded profile.
- No absorption of the emitted light to prevent artificial broadening by the stray light inside the material.
- Fast decay time, to enable the observation of possible variations of the beam size.
- Good mechanical properties for producing up to Ø100 mm large screens.
- Radiation hardness to prevent permanent damage.

For high intensity beams, one has to make sure that the material is not destroyed by the power absorption. A disadvantage of the screen is related to the interception. The used material is so thick (several mm) that it causes a large energy loss, so it can never be used for the diagnostics of a circulating beam inside a synchrotron. The screen is observed with a CCD camera. In older applications with video (i.e. analogue output), the digitalization is done with a frame grabber. A modern approach uses a digital link, with a digital data transfer of the CCD pixel values. In most cases, fiber optic links are used to get fast data rates and larger cable length without signal degeneration (see

[4] See https://www.crytur.cz/products/scintillation-screens

e.g.[5],[6]). A problem is the radiation sensitivity of the CCD sensor and the digital equipment. At high levels of radiation, the old-fashioned analogue VIDICON cameras are used.

For low-current beam diagnostics, scintillating crystals have larger signal-to-noise ratio than OTR screens or wire scanners (see below), and, therefore, are extensively used. For example, in accelerator AREAL YAG:Ce scintillation screens of 30 × 30 mm^2 and 20-μm thick are installed for profile measurements[7]. However, in Ref.[8], saturation of scintillating spots in the YAG:Ce crystal was noticed. Saturation becomes a relevant issue at beam intensities of the order of ~0.04 $pC/\mu m^2$ for a 100-MeV beam, and this limit scales with energy, being inversely proportional to the beam energy loss function.

The usage of few screen stations allows simultaneous determination of both the core region of the beam and its halo area[9] (see Fig. 5).

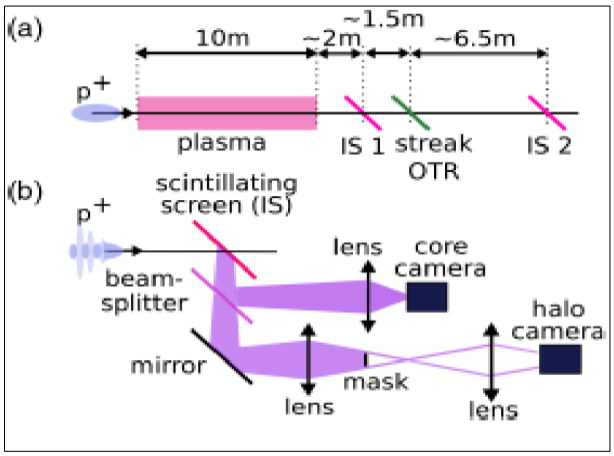

Fig. 5. (a) Schematic location of the imaging stations (IS1 and IS2) and of the OTR streak camera screen with respect to the plasma. The proton bunch moves from left to right. (b) Schematic drawing of the optical setup of the imaging station.

1.3. Secondary emission monitors (SEM)

When particles hit a surface, secondary electrons are liberated [1]. For the profile determination, individual wires or ribbons interact with the beam; this is called a Secondary Electron Emission grid or a harp. Each of the wires has an individual current-to-voltage amplifier. This is an electronic alternative to a scintillation screen with a much higher dynamic range i.e., the ratio of minimal to maximal detectable current is orders of magnitude larger.

For low energies at proton or heavy ion LINACs the particles are stopped in the material or undergo a significant energy loss. The ratio diameter-to-spacing of the wires determines the attenuation of the beam current (and of course also the signal strength on the individual wires). Typically, only 10 % of the beam area is covered by the wires and, in this sense, the profile measurement is nearly non-

[5] A. Peters P. Forck, A. Weiss, A. Bank, TRANSVERSE BEAM PROFILE MEASUREMENTS USING OPTICAL METHODS, Proc. Diag. Instrum. Part. Acc. Conf. DIPAC01, Grenoble, 2001, pp.123-125.
[6] R. Haseitl, C. Andre, F. Becker, P. Forck, BEAMVIEW - A DATA ACQUISITION SYSTEM FOR OPTICAL BEAM INSTRUMENTATION, Proc. PCs at Part. Acc. Conf. PCaPAC2008, Ljubljana, 2008, pp. 180-182.
[7] K. Manukyan, G. Zanyan, B. Grigoryan, A. Sargsyan, V. Sahakyan, G. Amatuni, BEAM DIAGNOSTICS FOR AREAL RF PHOTOGUN LINAC, Proceedings of International Beam Instrumentation Conference, IBIC2012, Tsukuba, Japan, (2012), pp. 212-214.
[8] A. Murokh, J. Rosenzeig, V. Yakimenko, E. Johnson, X.J. Wang, Limitations on the resolution of yag:ce beam profilemonitor for high brightness electron beam, The Physics of High Brightness Beams, pp. 564-580 (2000).
[9] M. Turner et al., Experimental Observation of Plasma Wakefield Growth Driven by the Seeded Self-Modulation of a Proton Bunch, PHYSICAL REVIEW LETTERS 122, 054801 (2019).

destructive. For energies above 1 GeV/u, the relative energy loss is negligible at single-pass accelerators and large size ribbons are used.

The SEM electronics have to be installed close to the accelerator hardware. With a multiplexer, the analog values are transported to an ADC located outside of the accelerator tunnel. Readout of a full SEM-grid usually takes less than a ms, which is typical for the use of pulsed or dc beams.

An interesting application for a profile measurement is the control of the injection into a synchrotron. If the orientation of the injected beam emittance is wrong due to a misaligned focusing, beam storage may still be possible, but can be improved with the help of diagnostics.

The SEM signal is typically used with low-energy beams as in this case no energetic secondary particles are generated for reliable measurement; this signal tends to be quite small and requires care in the acquisition. A serious problem with the detection of secondary emission is the fact that when the wire is heated above 1000 ^{0}C by the beam, it starts emitting electrons by thermionic emission perturbing the measurement of the SEM current [2].

1.4. Wire scanners

Another extensively used profiling method is scanning the electron or hadron beam with a thin wire (see reviews [2, 3, 4, 6, 8]). Information on the number of particles or photons that intersect the wire is determined by the intensity of the secondary particle or radiation flow generated by the interaction of primary particles with the wire material (see Fig. 6). The advantage of the method is the low impact of the measuring tool on the beam. Instead of using several wires with individual, expensive electronics, a single wire can be swept through the beam [1] (see also[10]). The advantage of wire scanning technique is also that the resolution is not limited by the wire spacing and therefore this technique is often used at electron accelerators with beam sizes in the sub-mm range. It can also be applied in proton synchrotrons due to the small amount of intercepting matter.

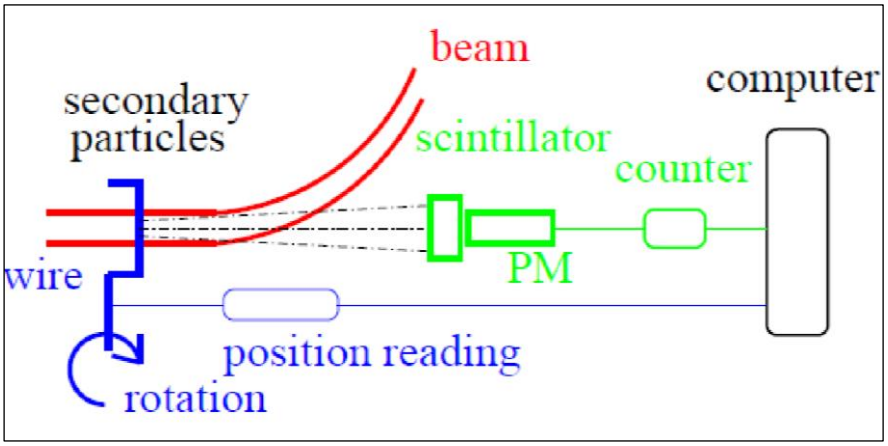

Fig. 6. Scheme of a wire scanner using the production of secondary particles as the signal source [1].

The disadvantage of wire scanning technique is that each scan provides information about only the one-dimensional profile of the beam (the wire integrates the contributions of all the particles along its length). In addition, for high-energy beams, the flow of secondary particles/radiation is directed along

[10] M. Plum, Interceptive Beam Diagnostics—Signal Creation and Materials Interactions, Beam Instrum. Workshop, Knoxville, 2004, AIP Conf. Proc. 732, p. 23.

the propagation direction of the measured beam and requires installation of an additional measurement system far from the interaction area, typically outside the vacuum chamber.

The signal from high-energy secondary particles is typically large due to the high gain of the scintillator/phototube detector. On the other hand, beam losses can pollute the signal and, more importantly, due to the geometry of the detector and of the beam line, the signal induced in the detector may depend on the position of the wire and direction of the particles, introducing distortions and aberrations in the profiles [2].

Different materials are used for the wires. The main criteria are mechanical strength and wire stability under the beam irradiation.

Silicon Carbide (SiC) coated carbon wires with diameters of 142 μm are used for the measuring wires in[11] (scanning wire monitors of ISIS Neutron and Muon Source, based at the Rutherford Appleton Laboratory). This material was noted as an ideal choice due to its rigidity and high emissivity, meaning it does not suffer from excess heating whilst intercepting the beam.

Scanning velocities up to 10 m/s can be achieved with a special pneumatic mechanism. Sometimes this setup is also called «flying wire» (see e.g. Fig. 7).

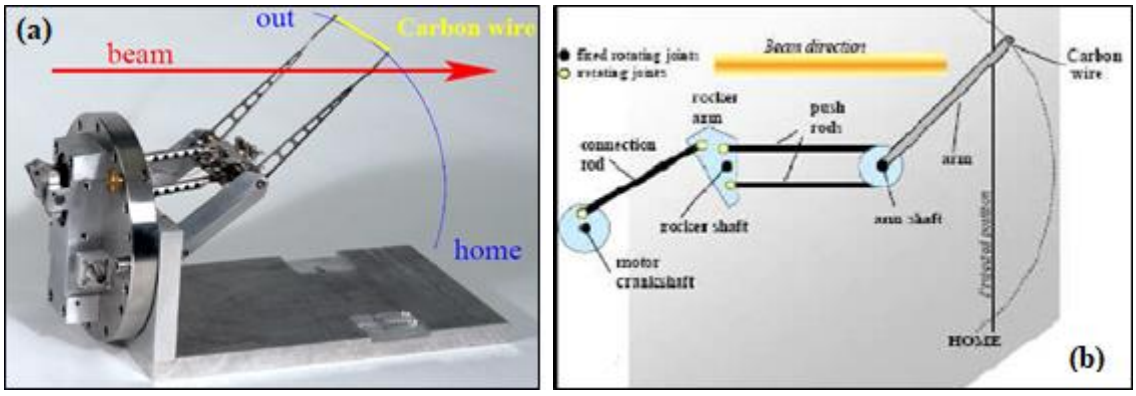

Fig. 7. (a) Pendulum scanner or «flying wire» used at the CERN synchrotron [1, 9]. (b) kinematic scheme of the scanner [2].

As the wire material, carbon or SiC is used due to its low weight and low nuclear charge Z, resulting in a low energy deposition in the wire [1]. These materials can withstand high temperatures without melting. The thickness can be down to 10 μm. But due to the scanned single wire and the high speed of the particles the profile is not taken at a single instant, even with high scanning velocity. Therefore, only the steady state distribution can be probed. For the display of the profile, the position of the wire, determined by the position encoder, is plotted on the horizontal axis. The beam signal for the vertical axis can be deduced from the current given by the emitted secondary electrons, like for a SEM-grid. This is done in particular for low energy protons and heavy ions. In most cases for beam energies larger than 150 MeV/u for ions (the threshold for π-meson production) or 10 MeV for electrons the signal is deduced by monitoring the secondary particles outside of the beam pipe (see Fig. 6). These secondary particles might be hadrons created by the nuclear interaction of the proton or heavy ion projectiles and the wire, having enough kinetic energy to leave the vacuum chamber. For the case of

[11] D. M. Harryman, C. C. Wilcox, An upgraded scanning wire beam profile monitoring System for the ISIS high energy drift space, 6th International Beam Instrumentation Conference, IBIC2017, Grand Rapids, 2017, pp 396-400.

electron accelerators, the secondary particles are mainly Bremsstrahlung-photons. The detector is just a type of well suited beam loss monitor, e.g. a scintillator installed several meters away. The count-rate is plotted as a function of the wire position as a precise representation of the beam profile.

Special fast wire scanners have been developed to decrease the scanning time (see e.g. [9, 10]) (speed of scan up to 20 m/s). Note the trend in the development of wire scanners with very short wires using nanofabrication technologies, designed to measure beams with sizes smaller than a few hundred microns [11, 12].

The superconducting CW LINAC, presently being commissioned at TRIUMF, will accelerate up to 10 mA of electrons to the energy of 30 – 50 MeV. Thus, average beam powers up to 0.5 MW are eventually expected. To support high beam power operation modes, a Fast Wire Scanner (FWS) capable of velocities up to 3 m/s over a 70 mm range was developed [10]. A stepper motor driven helical cam allows for a long stroke enabling two orthogonal wires to scan both axes in one scan. The radiation produced when the wires pass through the beam is detected by a BGO scintillator coupled to a photomultiplier (PMT), while the wire position is measured with a precision linear potentiometer.

Ref. [11] describes a new approach to wire scanners design based on nanofabrication technologies. This approach opens up new possibilities in term of wires shape, size, material and thickness with potential for even higher resolution and increased flexibility for instrumentation designers. The device, fabrication process and report measurement performed on the FERMI FEL electron beam are presented. An interesting investigation aimed to fabricate micrometer sizes wire scanners is reported in [12].

There was noted[12] that compared to view-screens monitor the beam profile wire scanners are normally immune to non-linear effects of the signal response and can perform high resolution measurements which ultimately depends on the wire diameter and scanning speed.

Wire scanners are considered as a good instrument especially for beam halo measurement [2] (see also[13],[14]).

Instead of measuring the flow of the scattered particles from the wire, a method has been developed to measure the secondary current generated by electron emission from the wire (see [2, 3] for an introduction to the method). In this case, the wire material must be conductive. The secondary emission signal is typically used with low-energy beams as in this case no energetic secondary particles are generated [2]. Monitors based on such principle usually named as Secondary emission monitors (SEM) are highly compact and require analogue measurements of small currents [1] (detailed review of this type of monitors see below).

---

[12] G.L. Orlandi, A. Alarcon, S. Borrelli, A. Gobbo, P. Heimgartner, R. Ischebeck, D. Llorente, F. Loehl, C. Ozkan Loch, P. Pollet, B. Rippstein, V. Schlott, First experimental results of the commissioning of the swiss FEL wire-scanners, 6th International Beam Instrumentation Conference IBIC2017, Ljubljana, Slovenia, 2017 pp 388-392.

[13] K. Wittenburg, DESY, MDI, Halo Monitoring: Very High Dynamic Beam Profile Measurements, Halo introduction.pptx, URL: https://www.google.com/url?sa=t&rct=j&q=&esrc=s&source=web&cd=1&cad=rja&uact=8&ved=2ahUKEwiN2_Dl6ubiAhUPcZoKHWYNARAQFjAAegQIABAC&url=https%3A%2F%2Fportal.slac.stanford.edu%2Fsites%2Fconf_public%2Fbhm_2014%2FPresentations%2FWittenburg%2C%2520Halo%2520introduction.pptx&usg=AOvVaw0Q9LzW-s1CN7vbb5TiF1Gh

[14] K. Wittenburg, Beam halo and bunch purity monitoring, URL: https://cas.web.cern.ch/sites/cas.web.../wittenburg-halo2.pdf.

A comparison of the wire scanner and the SEM-grid shows the advantages and disadvantages of both types:

- With a SEM-grid the beam intensity is sampled concurrently, whereas a moving wire samples the parts of the profile at different locations at different times. Therefore, variations of the beam intensity in time will be mixed with transverse intensity variations using a scanning device.

- In case of pulsed beams further complications may arise based on the need for exact synchronization, which can be easily solved in case of SEM-grid application.

- The resolution of a SEM-grid is fixed by the wire spacing (typically 1 mm), while a wire scanner can have much higher resolution, down to 10 μm, due to its constant movement. For high resolution, mechanical vibration has to be avoided.

- The electronics for data acquisition is cheaper for a scanning system. A SEM-grid requires one channel per wire.

- For the cost of the mechanics it is vice versa: The precise vacuum actuator for the scanner is more expensive than the pneumatic feed-trough needed for a SEM-grid.

For detailed descriptions of wire scanners for electron beam profiling see Ref. [8].

1.5. Multi-wire proportional chambers (MWPC)

For slowly extracted beams from a synchrotron, the current is much too low to be measured by a SEM-grid. One can use the amplification of electrons in a gas as done in a Multi-Wire Proportional Chamber MWPC. For the operation principle, see e.g. [1, 13]. The primary particles traverse a gas (like 90 % Ar mixed with 10 % CH_4 or CO_2), creating secondary electrons. A MWPC consists of a grid held at a high voltage, typically several kV, and a grounded grid, which is read by a charge-sensitive pre-amplifier, like for SEM-grids. The distance between the anode and the cathode plane is typically 1 cm and the spacing of the wires is about 1 mm. The principle is shown in Fig. 8. After reaching a threshold, the energy of the electrons accelerated toward the wires is high enough to knock out additional electrons from the gas atom/molecules. This gives rise to an avalanche, which results in a $\sim 10^4$ amplification of the number of electrons. This amplification inside the detector volume is nearly noise free due to the, electrically spoken, high source impedance of the free charge carriers. The resulting low noise could not be achieved by an electric amplifier due to its thermal noise. The following electronics (further amplifier and ADC) and the way of displaying is comparable to the procedure for SEM-grids.

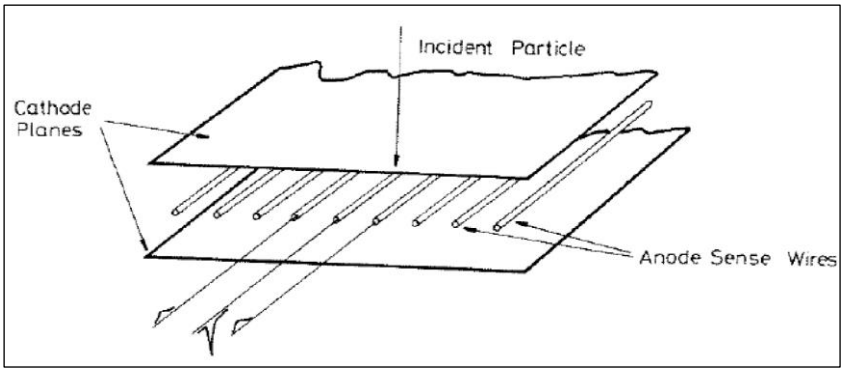

Fig. 8. The scheme of a MWPC for one plane showing the type of signal generating by a particle interaction [1].

1.6. Residual gas monitors

A frequently used non-destructive method for the profile determination is the Residual Gas Monitor RGM; it is sometimes also called Ionization Profile Monitor IPM [1]. The IPM is based on the interaction of the beam and the rest gas present in the vacuum chamber; even in the best vacuum there are still 10^{13} ions/cm^3 [2]. Such monitors are installed in nearly every proton/heavy ion synchrotron for the detection of beam sizes between some mm and several cm. For electron synchrotrons, they are not used so often, due to the smaller electron beam dimensions. The idea is to detect the ionized products from a collision of the beam particles with the residual gas atoms or molecules present in the vacuum pipe. Typical pressures for LINACs and transfer lines are in the range of 10^{-8}–10^{-6} mbar containing mainly N_2 and O_2 and for synchrotrons 10^{-11}–10^{-9} mbar containing mainly H_2. The different compositions are due to the different vacuum pumps used. A scheme for such a monitor is shown in Fig. 9. Due to electronic stopping, electrons are liberated and electron-ion pairs are generated. An estimation of the signal strength can be obtained by the Bethe-Bloch formula.

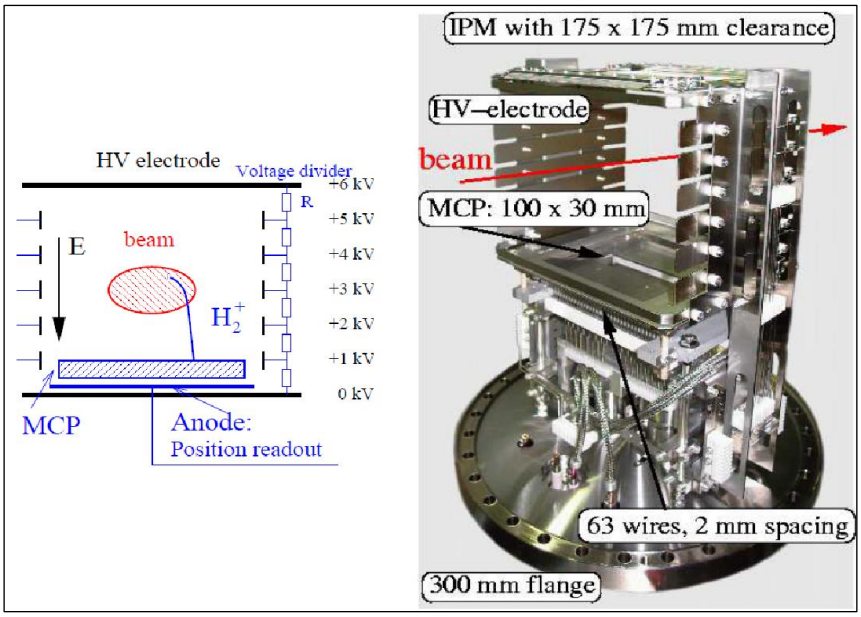

Fig. 9. Left: Scheme of a residual gas monitor for the horizontal profile determination. Right: The large aperture residual gas monitor installed at the GSI synchrotron for the horizontal direction. The clearance is 175×175 mm^2. The monitor is mounted on a Ø 300 mm flange. The read-out behind the MCP (bottom) is done with an array of 63 wires with 2 mm spacing [1].

The reconstruction technique of a two-dimensional beam density distribution through a residual gas ionization was initially proposed in the Kurchatov institute[15,16] (see also[17,18]).The concept of Beam

[15] V. Mihailov et al., General-purpose ionization detectors for accelerated particle beams, Instr. and Exp. Tech. 6 (1995) 39.
[16] S. Gavrilov, P. Reinhardt-Nickoulin, A. Titov, 2d non-destructive transverse diagnostics by beam cross-section monitors, 6th International Beam Instrumentation Conference IBIC2017, Ljubljana, Slovenia, 2017, pp 393-395.
[17] Ю.Г. Тетерев, А.Т. Исатов, С.В. Митрофанов, А.И. Крылов, Модернизация сканирующего двухмерного ионизационного монитора профиля в каналах транспортировки пучка, приборы и техника эксперимента, 6 (2020), 5–10.
[18] А.Т. Исатов, К.Д. Тимошенко, Л.А. Павлов, Обсуждение предварительных результатов: The Scanning Two-Dimensional Ionization Profile Monitor, 3-7 июня, 2024 г., Ереван.

Cross-Section Monitors (BCSMs) based on ion components of a residual gas ionization is presented in Fig. 10 (see also[19]).

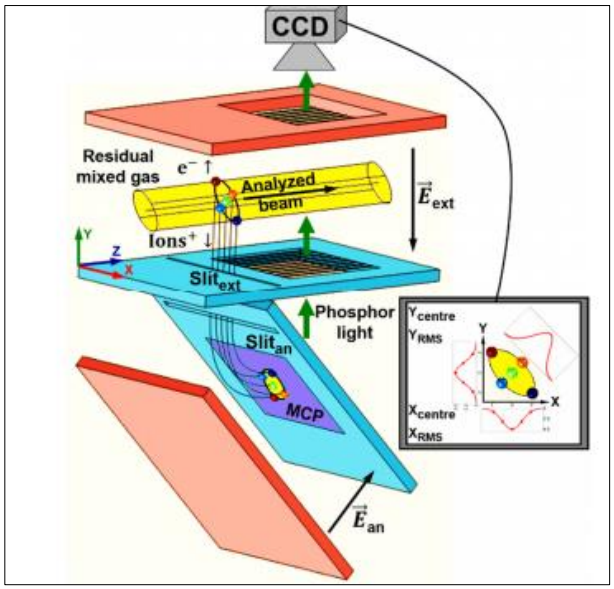

Fig. 10. Beam Cross-Section Monitor scheme.

Ionization profile monitors often suffer from artefacts in the measurement, the most important being the tails arising from the transverse drift of the electrons or ions during their travel towards the detector. More information on IPMs can be found in[20],[21].

Because of the low pressure of residual gas in some cases additional jet of O_2 can be used[22].

An interesting instrument is described in [6]. An ultrasonic 2-D jet of atomic Na (gas curtain) is produced in an oven followed by a collimation system. The Na-jet is inclined at 45° to the beam direction.

In[23] a special application of machine learning algorithms to the problem of reconstructing the actual beam profile from distorted measured profile is described.

1.7. Optical transition radiation monitors

Optical Transition Radiation (OTR) monitors are widely used for profile measurements at linacs. The radiation is emitted when a charged particle beam crosses the boundary between the two media with different optical properties (here a thin reflecting screen, e.g. a silicon wafer covered with a thin layer of aluminum or silver in vacuum) [7].

[19] S. Gavrilov, A. Feschenko, P. Reinhardt-Nickoulin and I. Vasilyev, Two-dimensional non-destructive diagnostics for accelerators by Beam Cross section Monitor, Journal of Instrumentation, V. 9, 2014, p. P01011.
[20] K. Satou, N. Hayashi, S. Lee, and T. Toyama, A prototype of residual gas ionization profile monitor for J–PARC RCS, 10th European Particle Accelerator Conference, EPAC2006, Edinburgh, UK, 2006, pp. 1163–1165.
[21] P. Forck, A. B. Bank, T. Giacomini, and A. Peters, Profile monitors based on residual gas interaction, 7th DIPAC, Lyons, France, 2005, pp. 223–227.
[22] Y. Hashimoto, Y. Fujita, T. Morimoto, S. Muto, T. Fujisawa, T. Honma, K. Noda, Y. Sato, S. Yamada, Chiba, Japan H. Kawauchi, A. Morinaga, Y. Taki, K. Takano, J. Takano, Development of a non-destructive beam profile monitor using a gas sheet, Proc. Part. Acc. Conf. PAC2001, Chicago, 2001, pp. 1631-1633.
[23] D. Vilsmeier, Space-charge distortion of transverse profiles measured by electron-based ionization profile monitors and correction methods, PHYSICAL REVIEW ACCELERATORS AND BEAMS 22, 052801 (2019).

When a fast electrically charged particle crosses the boundary between the two media of different dielectric constant, it emits so called Optical Transition Radiation. The effect is known since 1946, but its usage for beam diagnostics has become more widely spread only over the last decade[24].

With respect to scintillator screens, usually about 1 mm thick, OTR has the advantage of being obtained from very thin foils, with much less scattering of the beam particles, and therefore less emittance increase. OTR is emitted from both sides of the foil. Fig. 11 shows the situation at the entrance side.

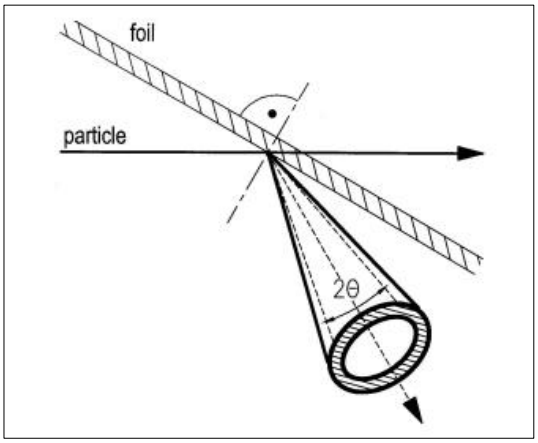

Fig. 11. OTR emitted from the entrance side of a foil. The radiation occurs into a hollow cone of opening-angle 2 θ around the «specular angle» (at which the particle would be reflected if it was a ray of light, and the foil a mirror), with $\theta = 1/\gamma$ of the particle [6].

In footnote[8] on page 6, different methods of profiling are compared. Scintillation YAG:Ce crystals of different thicknesses, an OTR screen, a phosphor screen, and a wire scanner (see also[25]) were used to measure the beam profile at the ATF photo-injector facility (a single-pulse photoelectron beam of 1 nC, with energy of 66 MeV). A significant sized blurring was observed on both YAG:Ce crystals and the phosphor screen compared to that on the OTR screen and wire scanner. The recorded results presented quite different full width at half maximum (FWHM) values: 380 μm for 0.5-mm YAG, 320 μm for 0.25-mm YAG, 300 μm for phosphor screen, 175 μm for the OTR screen, and 185 μm for the wire scanner (see also[26]).

1.8. Synchrotron radiation monitors

Synchrotron radiation is emitted when an electron beam is accelerated by electromagnetic fields. This occurs especially efficiently in a particle accelerator and has been observed first in a synchrotron. Synchrotron radiation is a good source of information; it is also there for the taking (although the taking may be quite expensive) [14]. For diagnostic purposes, the light is extracted from the accelerator and transported to the measuring equipment by means of various optical elements, such as windows, mirrors, lenses and fibers. The receivers are TV cameras, CCDs, photo diodes (single or in an array), etc.

[24] T.F. da Silva, Beam monitoring using Optical Transition Radiation, URL: http://beamdocs.fnal.gov/AD/DocDB/0036/003631/002/Chicago%20Presentation.pdf
[25] X.J. Wang, I. Ben-Zvi, J. Sheehan, V. Yakimenko, Brookhaven accelerator test facility energy upgrade, Proceedings 1999 Particle Accelerator Conference, New York, (1999), pp. 3495-3497.
[26] A.H. Lumpkin, B.X. Yang, W.J. Berg, M. White, J.W. Lewellen, and S.V. Milton, Optical techniques for electron-beam characterizations on the APS SASE FEL project, Nucl. Instrum. Meth. A, 429, pp.336-340, 1999

The information drawn may be simple, but very instructive, TV image of which enables to visually follow the evolution of the beam size; it may be a precise profile measurement; it may be a bunch length measurement with ps resolution which needs extremely fast oscilloscopes or a streak camera (that's where it gets expensive) [6].

An example of a synchrotron station is described in[27] (see Figs. 12, 13)

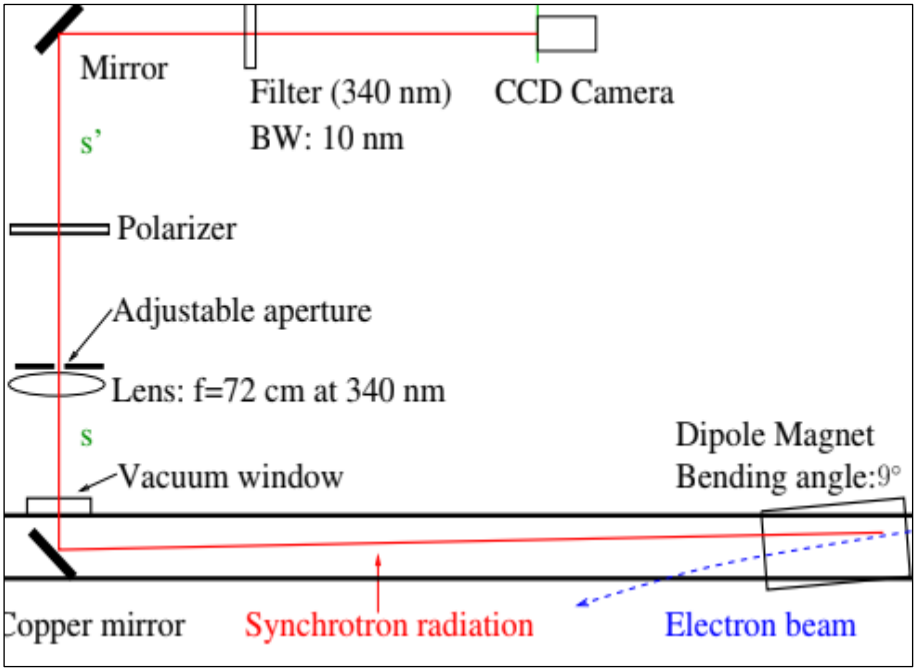

Fig. 12. The scheme of the transverse beam profile measurement system by synchrotron radiation. The direction of the synchrotron radiation is shown as a solid line (red), while the electron beam traverses a 9° dipole magnet along the dashed line (blue).

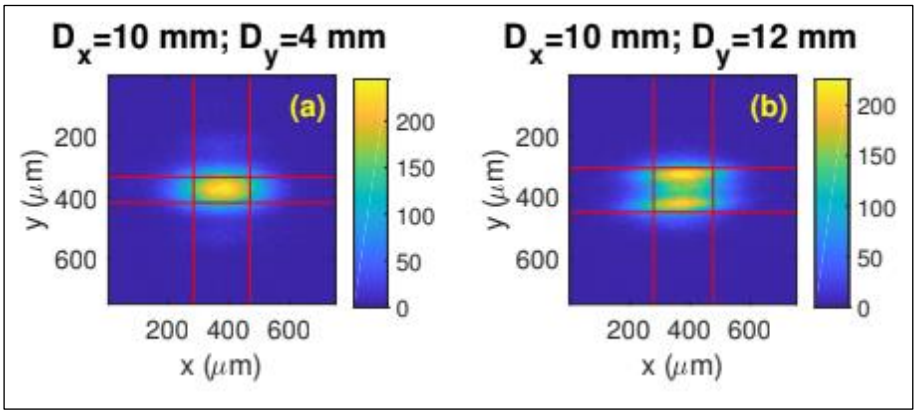

Fig. 13. Beam size measurements using the beam profile measurement system for a 0.1 mA single-bunch beam at 533 MeV. (a) and (b) are original images recorded by the CCD camera with horizontal aperture size D_x = 10 mm and the vertical aperture D_y = 4 mm or 12 mm, respectively.

Detailed description of an interferometer system and an imaging system using visible synchrotron radiation is presented in[28].

[27] B. Li, H. Hao, J.-Y. Li, Y. K. Wu, Transverse beam profile measurement system for the Duke storage ring, Nuclear Inst. and Methods in Physics Research, A, Volume 911, p. 45-50.

In[29] a technique for full reconstruction of the transverse beam profile based on a rotating double-pinhole mask is described.

1.9. Laser wire scanners

Another type of non-intercepting 1D pole monitor is the laser wire scanner. This device is based on the inverse Compton scattering (ICS) described before and is thus only available for electron and positron beams. The basic concept is quite simple and is depicted in Fig. 14. A powerful, well focused laser (referred to as the laser wire) is scanned across the beam to be measured, as is done in a traditional wire scanner. The photons of the laser interact with the high-energy electrons and create high-energy X-rays or γ-rays, with an energy boost of the order of γ^2. A detector downstream detects the flux of those particles [2].

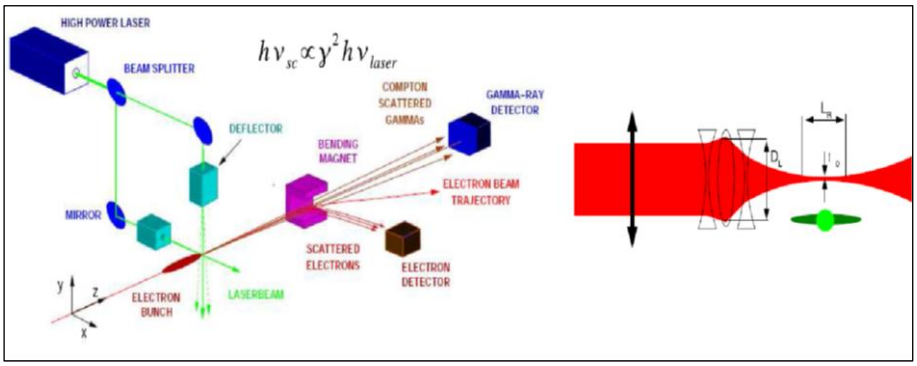

Fig. 14. The Scheme of a laser wire scanner system (left) and details of the laser focusing system (right) [2].

[28] K. TANG, B.-G. SUN, Y.-L. YANG, P. LU, L.-L. TANG, F.-F.WU, C.-C. CHENG, J.-J. ZHENG, H. LI, Transverse beam size measurement system using visible synchrotron radiation at HLS, arXiv: 1602.07918v1 25 Feb 2016, p.1-8.
[29] L. Torino and U. Iriso, Transverse beam profile reconstruction using synchrotron radiation interferometry, Physical review accelerators and beams, 19,122801 (2016).

2. Vibrating wire monitors for beam profile measurement [15]

2.1. Introduction

To address some of the limitations in the conventional beam instrumentation for accelerators, vibrating wire sensors and monitors have been developed since 1999 [16]. The operating principle of these sensors is based on the measurement of the change in the frequency of a vibrating wire as a function of the wire temperature. Instead of exciting traditionally used steel wires in the transverse vibration using an electromagnet, the interaction of the AC current through a vibrating wire with a permanent magnet is employed. This allows using non-steel wires and maintaining very stable wire oscillations (less than 0.005-Hz variation in a 5000-Hz full range). In accelerator diagnostics, vibrating wire monitors (VWMs) are mainly aimed at measuring the transversal profiles of different types of beams. The thermal principle of operation allows measuring charged particles, photons in a wide range of wavelengths, and even neutrons [17, 18]. It should also be noted that the inherent long-term reliability, minimum zero drift, and signal immunity to electrical noise are of prime importance [19].

The first instruments based on the vibrating wire technologies were developed in the late 1920s. Today the area of application of this technique expanded and different vibrating wire based sensors and monitors are used for measuring strain, displacement, piezometric level, pressure, angle and moment of rotation, viscosity of the media, and ultralow thermometry. The operating principle is based on the measurement of the change in the frequency of a vibrating wire depending on the physical parameters of the wire and environment in which oscillations take place. The advantages of properly constructed vibrating wire sensors are inherent long-term stability, high precision and resolution, good reproducibility and small hysteresis. The frequency signal of vibrating wire sensors is imperturbable and can be transmitted over long cable without degradation. It is also important to note a small zero drift and minimum change in sensitivity during a long time. An important parameter of vibrating wire-based sensors is their capability to operate in hard conditions[30],[31].

Original vibrating wire sensors and monitors for the beam instrumentation in accelerators were developed since 1999 [16] in Yerevan Physics Institute by group of accelerator diagnostics. The operating principle of sensors is based on the measurement of the change in the frequency of a vibrating wire depending on wire temperature. Instead of traditionally used steel wires excited into transverse vibration with the help of an electromagnet the interaction of AC current through the wire with a permanent magnet is used. This allows using non-steel wires and occurring very stable wire oscillations (less than 0.005 Hz in 5000 Hz full range). In accelerator diagnostics, vibrating wire monitors (VWM) are mainly aimed at measuring the transversal profile of different types of beams. The thermal principle of operation allows measuring charged particles, photons in a wide range of wavelengths and even neutrons [17, 18].

2.2. Physical fundamentals of vibrating wire method

2.2.1. Vibrating wire resonator and autogeneration principle

The operating principle of diverse vibrating wire sensors is based on the measurement of a change in the frequency of the vibrating wire that is stretched on a support, as a function of the physical

[30] D.M. Stefanescu, Handbook of force transducers: principles and components, Berlin : Springer-Verlag, 2011.
[31] A.J. Simmonds, Long term monitoring using vibrating wire sensors, Geokon Inc., Lebanon, NH, USA, 2015.

parameters of the wire and the environment in which the oscillations occur. There are numerous different types of vibration wire sensors (see e.g., [19]):

- In the permanent excitation method, an electrical energy impulse maintains sufficient energy in the wire for its permanent vibration.
- In the resonance method, typically two electromagnets are used. The first one acts as an actuator, whereas the second one serves as a sensor for the oscillation frequency observation.
- In the impulse method, an electromagnet serves as a shock actuator as well as a velocity sensor. An electrical impulse through an electromagnetic coil applies a very brief point force on the wire. After some time, the first mode component of the free response dominates.

As a background of the development, we use an electromechanical resonator with a vibrating metallic wire that is excited by the interaction of a current with a permanent magnetic field.

The automatic generation of vibrations at the natural frequency of the wire is achieved using a feedback electronic circuit (see below for more details) with a system for stabilizing the amplitude of the vibrations of the wire. This is important because a wire is essentially a nonlinear object, and its frequency can vary not only under the influence of the measured beam but also with the variations in the amplitude of the wire oscillations.

Advantages of the technology of permanent excitation of oscillations are noted in [19]; these include compactness of the magnets (leading to sensor volume reduction) and enhanced robustness. Our studies have shown that structures with permanent excitation of oscillations using magnets also have the following benefits. After a certain period when the sensor enters the operating mode, stable and flat single-harmonic oscillations are generated in the system. Simultaneously, the entire ensemble at the output of the autogeneration circuit continues to present the natural frequency of the wire oscillations, even under rapid variation.

A schematic of a typical vibrating wire resonator [20] is presented in Fig. 15. The resonator can be roughly represented as a support with a strained vibrating wire. Special clamps rigidly fasten the ends of the wire, so that its length is strictly defined by the distance between these clamps (the base is much more rigid than the wire).

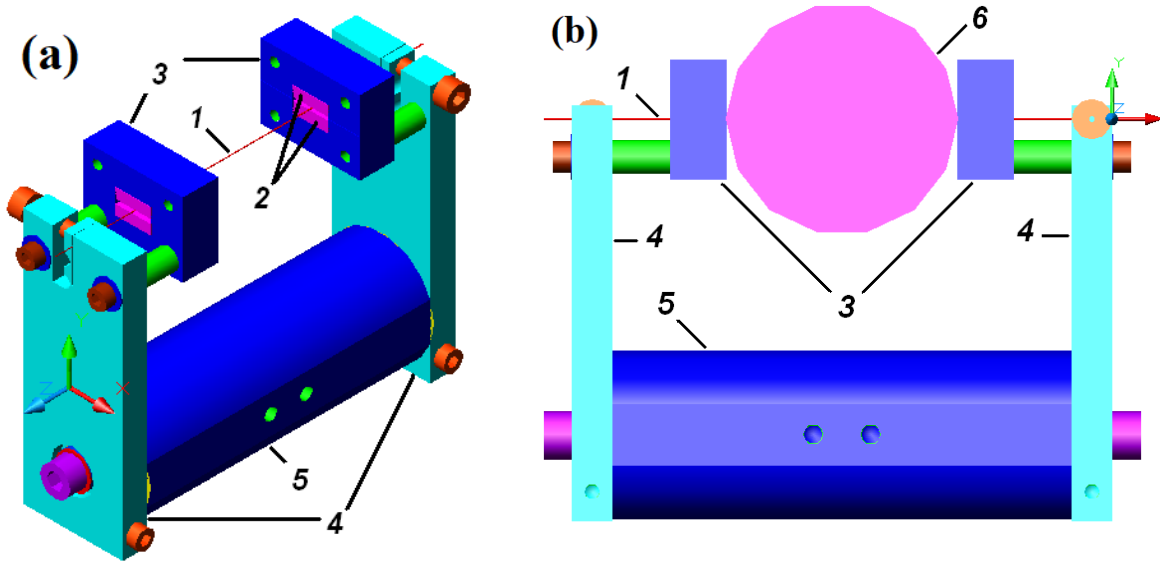

Fig. 15. (a) Main view of monitor with aperture of 40 mm and wire length of 80 mm: 1 – vibrating wire, 2 − magnets, 3 − magnet poles, 4 − clamps, 5 − basis. (b) Aperture of monitor is defined by circle 6 placed between magnet poles.

The scheme of the autogeneration of natural oscillations of the wire is presented in Fig. 16. The basis of the oscillation generation process is the amplification of the random vibrations of the wire. The wire is connected to a positive feedback circuit, so that the mechanical fluctuations on the wire generate an electromotive force (emf) pulse that is amplified and transmitted to the wire in the same phase. Because the attenuation of the oscillations is minimal in response to the natural frequency of the circuit, the resonant frequency that is selected by the feedback circuit is equal to the natural frequency of the wire. The electrical signal from the wire is actually that at the output of the operational amplifier in the feedback circuit (OP1 output in Fig. 16). We also added an important system for stabilizing the amplitude of the generated oscillations.

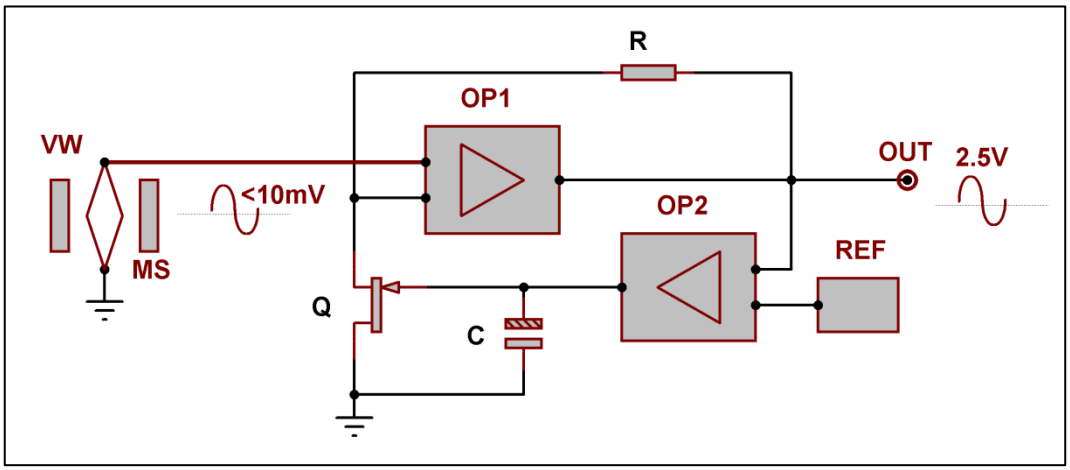

Fig. 16. Automatic generation board of natural oscillations of wire (schematically). VW - vibrating wire, MS - magnetic system, OP1 - main operational amplifier unit, OP2 - operational amplifier unit in wire oscillation amplitude stabilization circuit, REF - voltage reference source that regulates oscillation amplitude, Q - field transistor in circuit of wire vibration amplitude stabilization, OUT - output signal, R - resistor, whose nominal value is selected depending on parameters of resonator, C – capacitor that adjusts process of signal stabilization depending on frequency range of oscillations.

The process of autogeneration is complex and defined by all the parameters of the sensor resonator as well as the circuit and values of the electronic components in the scheme of autogeneration. The former are the diameter and length of the wire, material of the wire, structure of the magnetic field including the distribution of the magnetic field along the wire, and value of the magnetic field in the area of the wire. The magnetic field is determined by the type of permanent magnets used and the size of the magnetic pole gap. Accordingly, the process of starting vibrations at the natural frequency is significantly different for different types of sensors. It should be noted that in [21], the resonator, consisting of a vibrating wire, its mounting system, and the magnetic field, is interpreted as an equivalent electrical circuit comprising an inductor, a resistor, and a capacitor (see also[32],[33],[34]). Such a

[32] P.L. Woodfield, A.D. Seagar, Viscous Drag Force and Heat Transfer from an Oscillating Micro-Wire, Proceedings 18th Australasian Fluid Mechanics Conference, Launceston, Australia, 3-7 December 2012
[33] J.T. Tough, W.D. McCormick, J.G. Dash, Vibrating Wire Viscometer, Rev. Scientific Instruments, 35, 1964, 1345-1348.
[34] L. Bruschi, M. Santini, Vibrating Wire Viscometer, Rev. Scientific Instruments, 46, 1975, 1560-1568

replacement of the resonator by an equivalent unit of electronic components allows to effectively select component values of the autogeneration scheme (see Fig. 17).

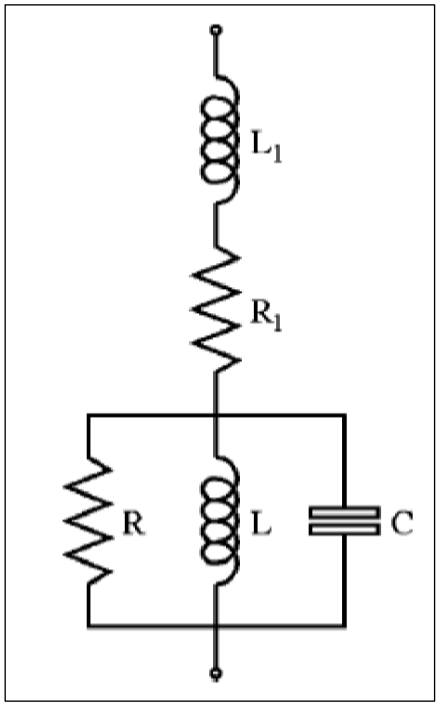

Fig. 17. Electronic lumped-parameter RLC circuit equivalent to vibrating wire resonator [21] (a parallel RLC oscillating circuit can be considered an electrical analog of the mechanical oscillator, in which R_1 and L_1 describe electrical properties of the wire and leading-in cable).

2.2.2. Resonator and magnetic field selection

The selection of the vibrating wire resonator is governed by the specific application of the monitor. The standard VWM consists of a single wire, wire clamps, and a magnetic field system, as shown in Fig. 15. The space along the wire is almost half occupied by the magnetic field, which reduces the aperture of the sensor. In some cases, resonators with the largest possible aperture are required, to measure beams with a large transverse beam size. For this purpose, several variants of such large-aperture monitors have been developed on the yoke principle [22, 23, 24]. This type of a VWM has two mechanically coupled wires (vibrating and target). Coupling is maintained by a special balancing arm (yoke). Such a monitor has a much larger aperture size than previous VWM models. A prototype of such a large-aperture VWM with a target wire length of 60 mm was designed, manufactured, and bench-tested on a proton beam of Fermilab High Intensity Neutrino Source facility (with proton energy of 2.5 MeV and average beam current of 0.01–2.8 mA [23]) (see Fig. 18).

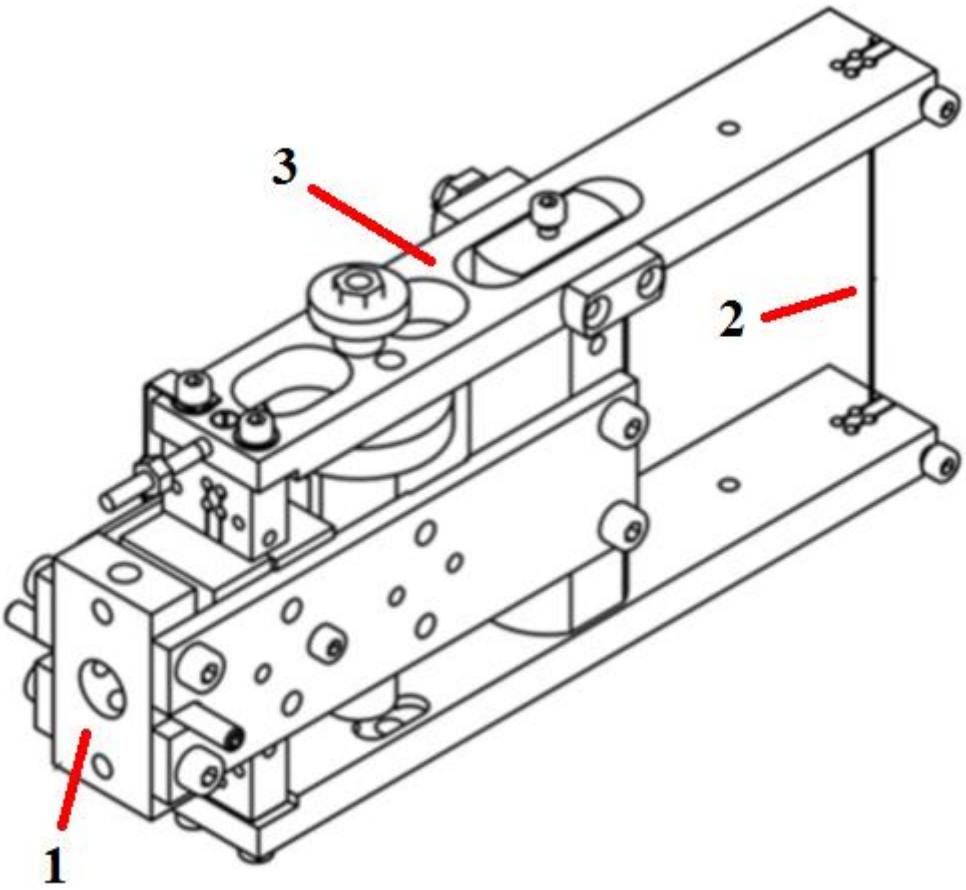

Fig. 18. Yoke-type vibrating wire resonator: 1 – vibrating wire assembly, 2 – target wire, 3 – balancing arm (yoke) coupling vibrating and target wires.

Multi-wire sensors with a system of vibrating wires have also been produced. Such sensors allow measurement of a beam profile at the corresponding number of points without scanning the beam. Monitors with five wires were manufactured and used to measure the undulator and synchrotron radiations at the Advanced Photon Source of Argonne National Laboratory (APS-ANL) [25, 26] (see below for more details).

For some applications (e.g., for thin-beam profiling, where the vibrating wire plays the role of a miniature scanner), it is desirable to increase the amplitude of the oscillation of the wire, i.e., to increase the sweeping area of the wire during its oscillation. This could be realized by increasing the autogeneration current in the oscillation excitation circuit. However, this is not desirable, because of the consequent increase in the degree of nonlinearity in the oscillations of the wire. For the development stage of the method of thin-beam profiling using a vibrating wire [27, 28], the sinusoidality of the oscillations needs to be maintained, which would permit precisely defining the position of the wire in space. Therefore, as an alternative, we increased the length of the wire. A model resonator with a length of 120 mm and a movable magnetic field system was developed. The design of such a resonator with a magnetic field created by a pair of magnetic poles (11 mm in width) with permanent magnets of diameter 10 mm and thickness 5 mm is shown in Fig. 19(a). Specifically, the resonators discussed here are aimed at the excitation of the flat oscillations of a wire. The problem is that the frequencies of natural vibrations in two orthogonal transverse directions differs slightly, because of ovality of the wire and asymmetry in the fastening at its ends. Nonflatness of the

oscillations may arise, owing to the defects in the manufacturing and alignment of the magnetic system components. For studying completely mixed oscillations in transverse directions in this resonator, it is possible to rotate two units of the magnetic system by 90° from each other (see Fig. 19(b)).

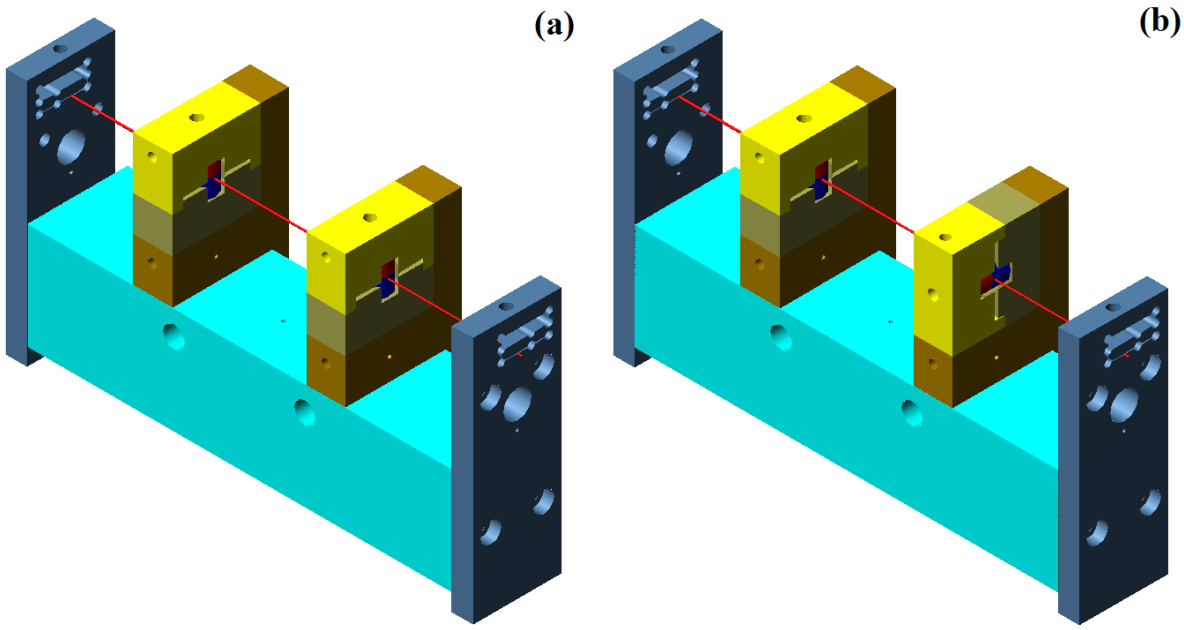

Fig. 19. Vibrating wire resonator design with wire length of 120 mm for studying influence of magnetic system on wire oscillations: (a) planes of two units of magnetic system coincide, (b) planes of two units are orthogonal to each other.

Note that in resonators in which the magnetic field covers only a small part of the length of the wire, there is a probability that several harmonics may be excited simultaneously. For the resonator shown in Fig. 19(a), the distribution of the magnetic field is presented in Fig. 20. As can be seen, this arrangement of magnetic poles practically excludes the generation of the third-harmonic oscillations; however, it is favorable for the excitation of the first and fifth ones i.e., oscillations tend to be excited if the magnetic field and the corresponding force on the wire are concentrated in the region of oscillation antinodes, and conversely if the magnetic field is concentrated near oscillation nodes, oscillations are not easily excited.

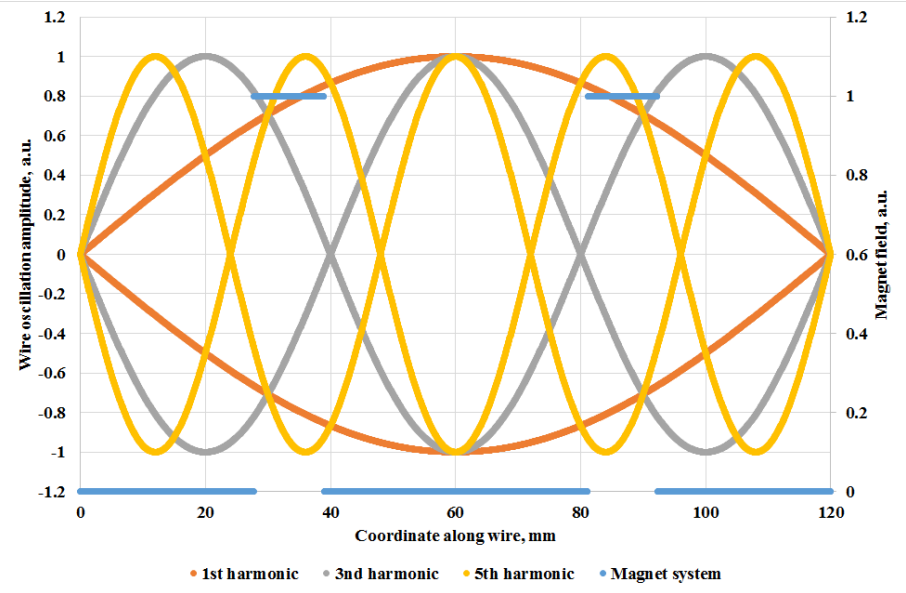

Fig. 20. Magnetic field and oscillation harmonics of vibrating wire resonator with length of 120 mm. Blue line - distribution of magnetic field along wire, orange – first-harmonic oscillations of wire, grey – third-harmonic oscillations, yellow – fifth-harmonic oscillations.

Below are some results obtained using a model resonator with a 120-mm wire length for various modification of the autogeneration boards. The measurements were made with a RTB2004 oscilloscope. The results of the autogeneration process of the natural oscillations for the StrGen DVW_2018 board with operational amplifiers in the SMD version and capacitor C = 3300 nF (see Fig. 16) are presented in Fig. 21. An interesting feature was noted: the autogeneration process began with the generation of the fifth-harmonic oscillation, which after a reasonably long time (approximately 10 s) was regenerated in the production of the first harmonic in the form of an admixture of oscillations. The fraction of the fifth harmonic depended on the features of the electronic components of the autogeneration board and the values of the key resistors and capacitors.

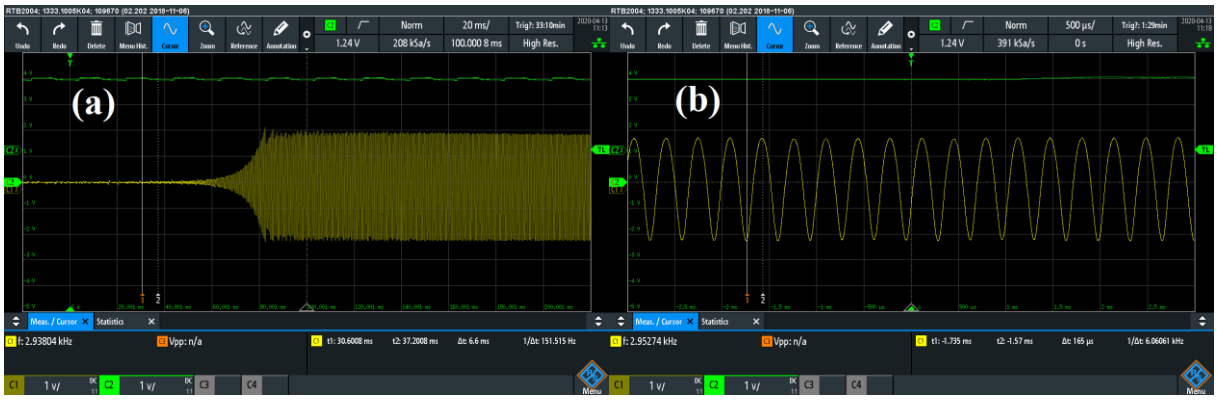

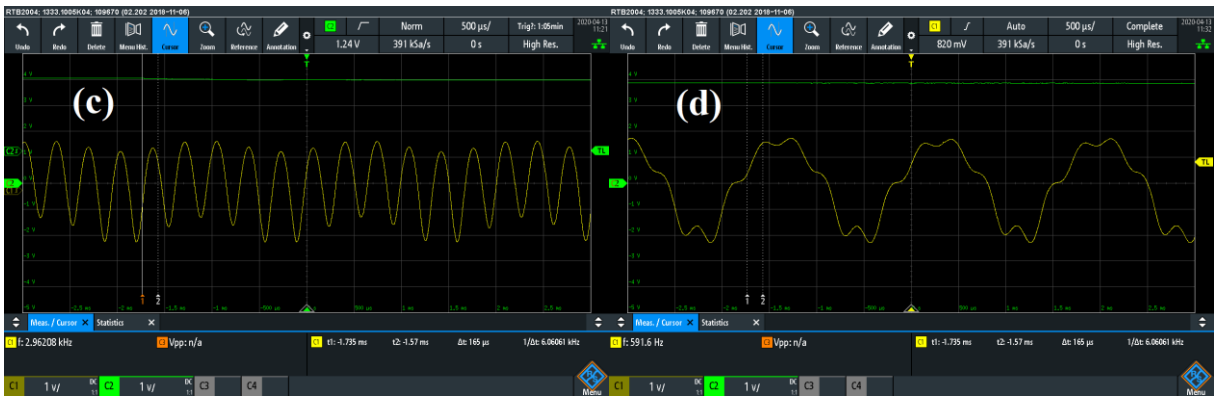

Fig. 21. Autogeneration process using 120-mm wire length monitor, autogeneration board StrGen DVW_2018 with operational amplifiers in SMD version, and capacitor C = 3300 nF. (a) Because of high capacitor values in feedback circuit, autogeneration process starts after approximately 3 s, and the fifth harmonic is generated. Horizontal scale of the oscilloscope waveform is 20 ms per division. (b) Fifth harmonic sustains for sufficiently long time (up to 5 s). Horizontal scale of the oscilloscope waveform is 500 µs per division. (c) Subsequently, together with the fifth harmonic, first harmonic (12 s) increases. Horizontal scale of the oscilloscope waveform is 500 µs per division. (d) System enters stationary mode (over 30 s), with a mixture of first and fifth harmonics, in which fifth harmonic is important. Horizontal scale of the oscilloscope waveform is 500 µs per division.

Fig. 22 shows a similar process of oscillation generation of the same resonator with an StrGen V4.1USB board, which used operating amplifiers in the DIP version and capacitor C = 220 nF.

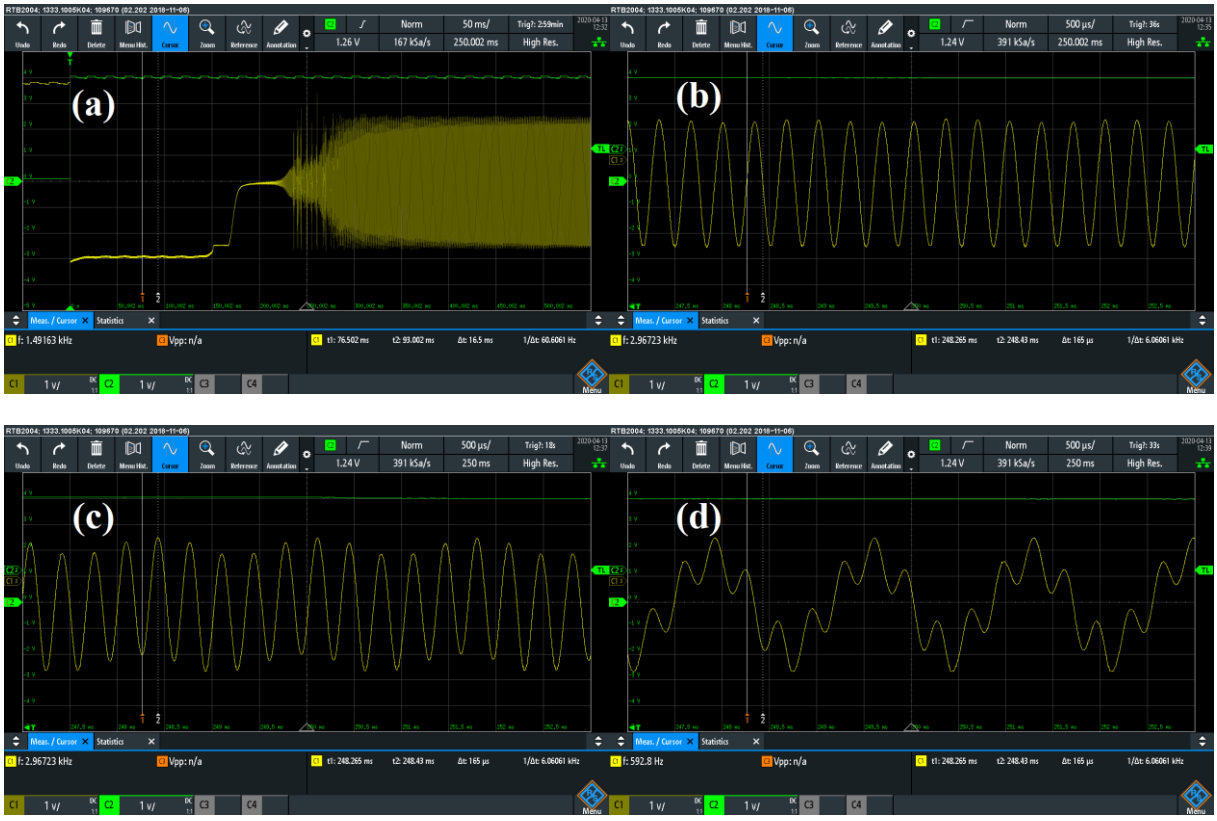

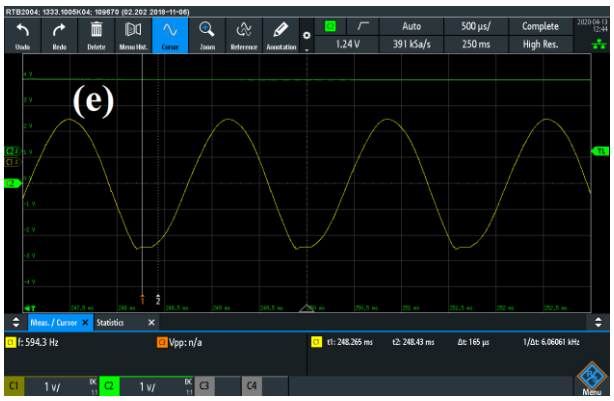

Fig. 22. Autogenerationprocess using 120-mm wire length monitor, autogeneration board StrGen V4.1USB with operating amplifiers in DIP version, and capacitor C = 220 nF. (a) Because of low capacitor values, the generation process starts early. Horizontal scale of the oscilloscope waveform is 50 ms per division. (b) Similar to previous case, initially fifth harmonic is generated. Horizontal scale of the oscilloscope waveform is 500 µs per division. (c) Appearance of fifth harmonic after 1 s. Horizontal scale of the oscilloscope waveform is 500 µs per division. (d) Subsequently, first harmonic starts to increase (5 s). Horizontal scale of the oscilloscope waveform is 500 µs per division. (e) After 10 s, the first harmonic sustains, with slight distortion of sinusoidal oscillations near extremes, probably due to admixing of fifth harmonic. Horizontal scale of the oscilloscope waveform is 500 µs per division.

2.2.3. Frequency dependence on wire temperature

The interaction of the beam with the wire mainly causes the wire to heat. The corresponding change in the natural oscillation frequency of the wire provides information about its temperature and accordingly the number of particles/photons of the beam penetrating the wire.

At the assembly temperature (T_0), the tension of the wire is defined using the length between the clamps mounted on the base, L_B^0 (bed length) and the non-tensioned wire length, L_W^0 as follows:

$$\sigma_0 = \frac{L_B^0 - L_W^0}{L_W^0} E_W = \frac{\Delta L_W^0}{L_W^0} E_W , \qquad (1)$$

where E_W is the elasticity modulus of the wire material.

The frequency of the second harmonic of the wire oscillations can be expressed as

$$F_0 = \frac{1}{L_B^0} \sqrt{\sigma_0 / \rho} , \qquad (2)$$

where ρ is the density of the wire material.

Let us assume that the wire is heated by ΔT (ambient temperature and temperature of the base remain unchanged). The corresponding change in the wire density yields

$$\frac{\Delta\rho}{\rho} = -3\alpha_W \Delta T\,, \tag{3}$$

where α_W is the linear expansion coefficient of the wire.

Because the length of the wire is determined by the distance between the attachments points on the base (bed length), it is L_B^0 and does not change. However, the tension in the wire varies, owing to changes in the length of the wire in the non-tensioned state. We have

$$\frac{\Delta L_W}{L_W^0} = \alpha_W \Delta T\,, \tag{4}$$

and correspondingly,

$$\Delta\sigma = E_W \frac{L_W^0}{L_B^0} \alpha_W \Delta T\,, \tag{5}$$

and accordingly,

$$\frac{\Delta\sigma}{\sigma_0} = \frac{E_W}{\sigma_0} \frac{L_W^0}{L_B^0} \alpha_W \Delta T\,. \tag{6}$$

The process of tensioning the wire when only its temperature changes is illustrated in Fig. 23.

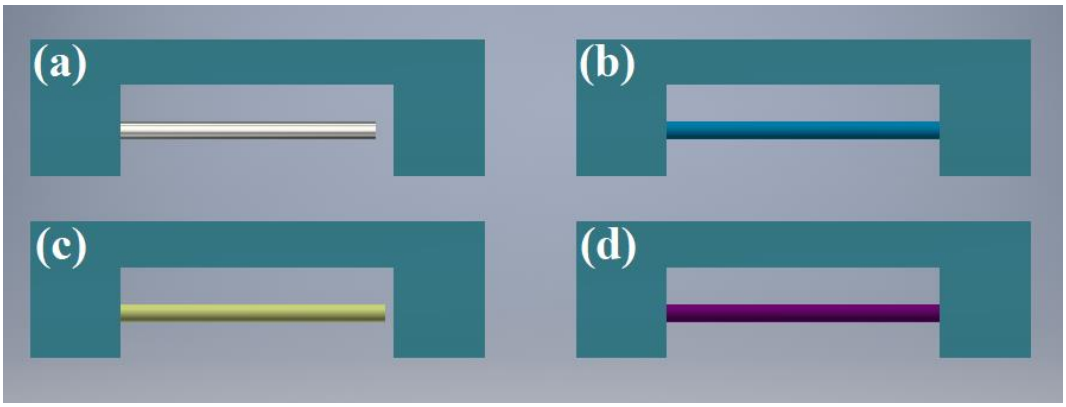

Fig. 23. Tensioning wire when only its temperature changes. (a) Base (cadet blue) - length of bed for wire L_B^0 = 30 mm, wire (silver) - length in non-tensioned state L_W^0 = 28 mm. (b) Wire (sky blue medium) is stretched on bed length of base and becomes L_B^0 = 30 mm, i.e., tension of wire is calculated using ΔL_W^0 = 2 mm. (c) For base, temperature does not change, i.e., bed length remains 30 mm, whereas on heating, length of wire (satin lemon chiffon) in non-tensioned state increases to $L_W = L_W^0(1+\alpha_W \Delta T)$ = 29 mm. (d) Wire (smooth purple) is stretched along bed length of base and becomes 30-mm long, i.e., wire tension is calculated using ΔL_W = 1 mm.

The values of the expansion coefficients of metals are in the range of a few units of 10^{-6} - 2×10^{-5} K^{-1} Thus, at a temperature shift of 1 K, the relative changes in both the length and density are

approximately 10^{-5}. Under tension, based on Eq. (6), there is an additional factor, E_W / σ_0, which is very large. For example, for stainless steel (AISI 316), E_W = 190–210 GPa and the tensile strength is 460–860 MPa. The initial tension on the wire was taken as 30%–70% of the tensile strength (assumed to be 700 MPa for the VWM wire), so that E_W / σ_0 is approximately 400. From these simple estimations one can see that the temperature dependence of ρ is negligible compared to that of the tension. As a first approximation, one can also neglect the difference between L_B^0 and L_W^0, so that without causing any misunderstanding we can use $L_W^0 \approx L_B^0 \approx L$. To summarize, we obtain

$$F = \frac{1}{L}\sqrt{(\sigma_o - E_W \alpha_W \Delta T)/\rho}\,. \qquad (7)$$

Fig. 24 presents the temperature dependence of the frequency and sensitivity of the resonator utilizing the vibrating wire.

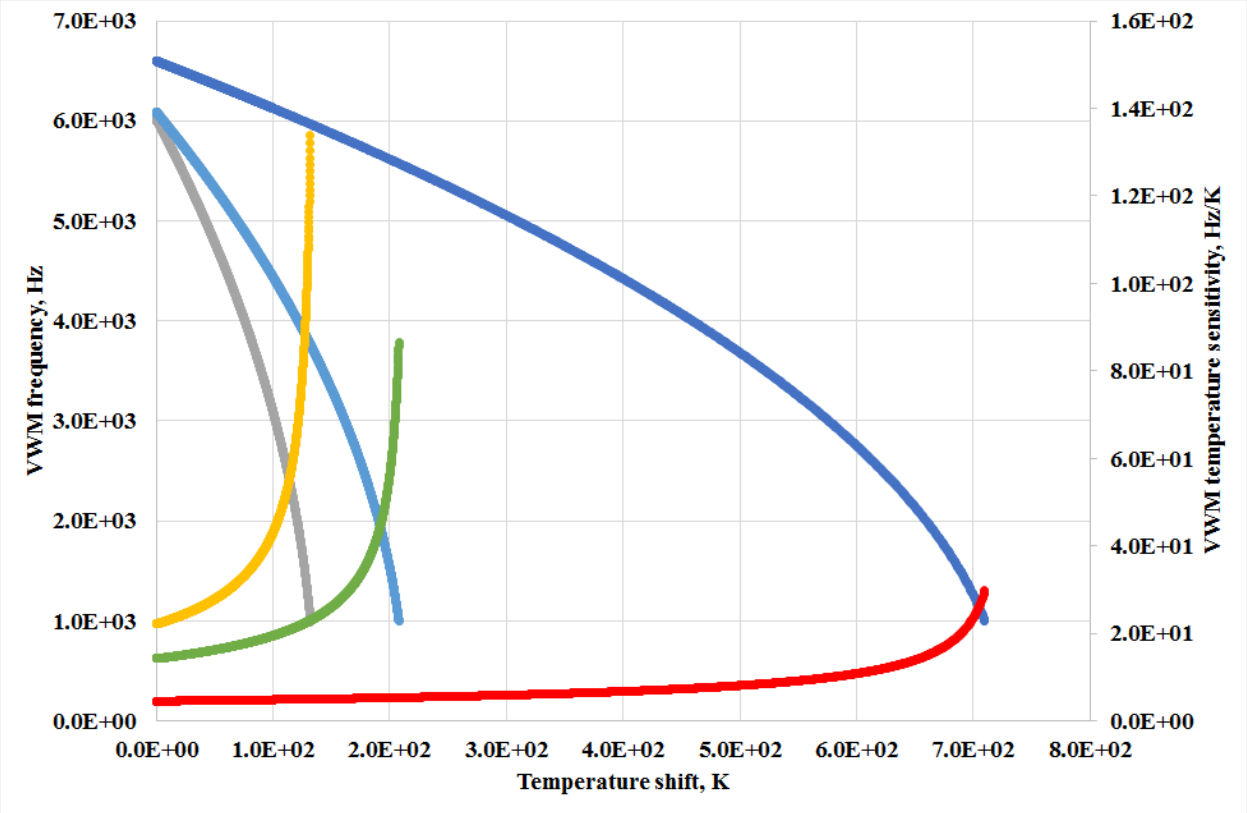

Fig. 24. Frequency of vibrating wire and sensitivity of monitor to overheating of wire as functions of temperature of assembly with wires formed of tungsten (frequency – dark blue, sensitivity - red), beryllium bronze (Beryllium Bronze - Cu97.5/Be2/Co-Ni0.5, UNS C17200) (frequency – blue, sensitivity - green), and stainless steel (AISI 316) (frequency – gray, sensitivity - yellow). Sensitivity of monitor is slope of frequency versus temperature relation. In all three cases, it is assumed that during assembly, wire is stretched by 70% of the strength of material.

Table 1 contains mechanical parameters of wire materials (for tungsten and stainless steel, data are taken from[35] and for bronze from[36]), and values of initial tension and corresponding frequency of VWM.

Table 1. Mechanical parameters of some wire materials and corresponding initial characteristics of VWM. Here, σ_{TS} is the tensile strength.

	E_W, GPa	σ_{TS}, MPa	ρ, kg/m^3	α_W, K^{-1}	$\sigma_0 = 0.7\sigma_{TS}$, K^{-1}	F_0, Hz
Tungsten	411	1920	19.2×10^3	4.5×10^{-6}	1344	6597
Stainless steel	190-210	460-860	7.96×10^3	$(16\text{-}18)\times10^{-6}$	462	6023
Beryllium bronze	131	700	8.26×10^3	17.5×10^{-6}	490	6089

As the upper limit of the wire temperature range, in Fig. 10, we set the value as that corresponding to where the frequency drops to 1000 Hz, below which the autogeneration system typically does not provide a stable process of oscillation generation.

2.2.4. Frequency dependence on ambient temperature

VWMs are also affected by the ambient temperature. Let us consider that the wire is also exposed to a local heat source. For certainty, we introduce the following three temperatures:

$T_A(t)$ - ambient temperature,

$T_B(t)$ - temperature of the VWM base,

$T_W(t)$ - temperature of the VWM wire.

We assume that the ambient temperature variation is sufficiently gradual, so that

$$T_A(t) = T_B(t). \tag{8}$$

In addition, the temperature of the wire is divided into two components: the ambient temperature and the excess over this temperature due to the local source that only affects the wire. Therefore,

$$T_W(t) = T_A(t) + T^{ag}(t). \tag{9}$$

In fact, we neglect the low flow of heat from the wire to the clamps and base, noting their heat capacity difference and poor heat transfer by contact.

At the start of the experiment (t = 0),

$$T_A(0) = T_B(0) = T_W(0) = T_0, \tag{10}$$

where T_0 is the initial temperature, and at measuring time t,

[35] See in https://www.goodfellow.com/
[36] See in http://www.matweb.com/search/datasheet.aspx?matguid=ff8cccd594eb46afbe82d15bf06e

$$F(t) = \frac{1}{L}\sqrt{(\sigma_o + E_W(\alpha_B - \alpha_W)(T_A(t) - T_0) - E_W\alpha_W T^{ag}(t))/\rho}\,. \qquad (11)$$

As can be understood, the frequency response accumulates the signal of the wire temperature change and is also subject to the ambient temperature changes (in the case of a long-duration experiment, this will be perceived as a drift in the initial frequency).

The process of wire stretching when the ambient temperature changes in addition to the heating from the beam impact (local source) is schematically shown in Fig. 25.

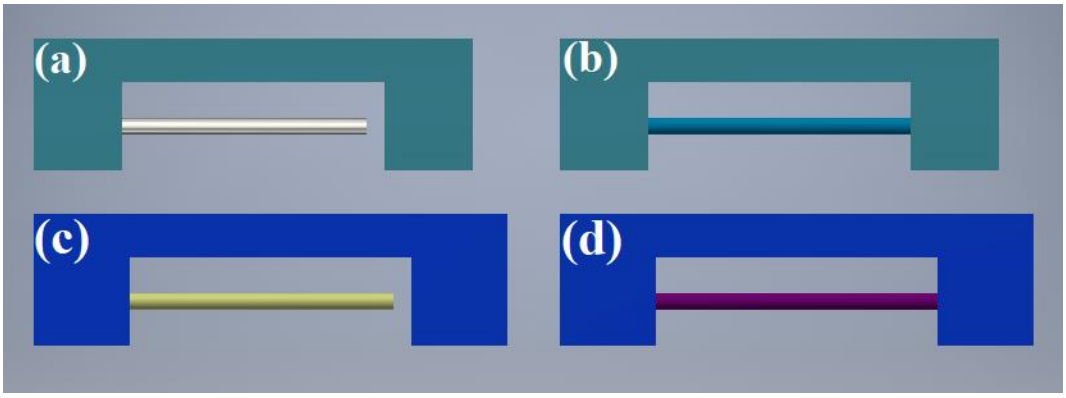

Fig. 25. Tensioning wire when ambient temperature changes, as well as additional heating from beam impact. (a) Base (cadet blue) - length of bed for wire L_B^0 = 30 mm, wire (silver) - length in non-tensioned state L_W^0 = 28 mm. (b) Wire (sky blue medium) is stretched on bed length of base and becomes L_B^0 = 30 mm, i.e., tension of wire is calculated using ΔL_W^0 = 2 mm. (c) Base (clear blue) - as ambient temperature changes, bed length becomes $L_B = L_B^0(1+\alpha_B\Delta T)$ = 32 mm, whereas wire (satin lemon chiffon) length in non-tensioned state increases to $L_W = L_W^0(1+\alpha_W\Delta T)$ = 29 mm, on heating. In addition, wire is also heated by additional source, i.e., measured beam. Thus, total length of non-tensioned wire becomes $L_W = L_W^0(1+\alpha_W(\Delta T + \Delta T^{ag}))$ = 30 mm. (d) Wire (smooth purple) is stretched along bed length of base and becomes 32 mm, i.e., wire tension is calculated using ΔL_W = 2 mm.

One can see that in the specific case

$$\alpha_B - \alpha_W = 0\,, \qquad (12)$$

the frequency does not depend on the ambient temperature. We call this type of sensor a temperature-compensated VWM. However, one should note that this compensation occurs only for very slow processes.

2.2.5. VWM with reference wire

An alternative approach is to manufacture a sensor with two vibrating wires: one is exposed to the beam, and the second one is used as reference for considering the gradual changes in the ambient temperature (see Fig. 26).

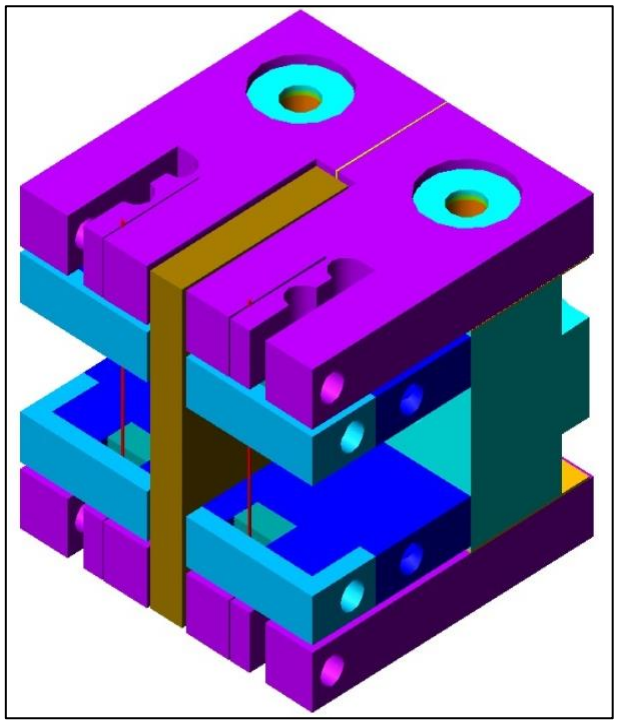

Fig. 26. Double-wire vibrating wire monitor (DW-VWM).

In this case, the VWM consists of two identical wires on a common base. One wire (first, with temperature $T'_W(t)$) is exposed to the beam; the other (second, with temperature $T''_W(t)$) serves as a reference. For the second wire, we assume $T''_W(t) = T_A(t)$. As in the previous case, we divide the temperature of the first wire into two components: ambient temperature and the impact of a local source that acts only on the first wire. To determine this impact, we have two equations:

$$F'(t) = \frac{1}{L}\sqrt{(\sigma_o + E_W(\alpha_B - \alpha_W)(T_A(t) - T_0) - E_W\alpha_W T^{ag}(t))/\rho}, \quad (13)$$

$$F''(t) = \frac{1}{L}\sqrt{(\sigma_o + E_W(\alpha_B - \alpha_W)(T_A(t) - T_0))/\rho}. \quad (14)$$

From these equations, one can finally obtain

$$T^{ag}(t) = \frac{L^2\rho}{E_W\alpha_W}\left[\left((F''(t))^2 - (F''_0)^2\right) - \left((F'(t))^2 - (F'_0)^2\right)\right]. \quad (15)$$

2.2.6. Thermal balance of VWM

The beam penetrating the wire loses some energy and heats the wire. The wire temperature increase relative to its initial temperature can be calculated by the equation of balance between the power deposited in the wire and the heat sink through all possible thermal mechanisms. These mechanisms are conduction along the wire to the end clips, convection losses to the ambient atmosphere (if air or another gas is present), and losses through the radiation to the ambient space. It is assumed that there are no other heat sources except the beam impact, and that the profile of the balanced temperature has a triangle profile along the wire (i.e., at the wire ends we set the temperature to T_0 , and at the middle

to the maximal temperature T_{MAX}). This approximation is ~~a~~ sufficiently close to real temperature profile along the wire. The balance equation is written as

$$W_{beam} = W_{\lambda} + W_{rad} + W_{conv}, \tag{16}$$

where W_{beam} is the deposited power from the beam into the wire,

$$W_{\lambda} = 8(T - T_0)\lambda S / L \tag{17}$$

is the conductive heat sink,

$$W_{rad} = \varepsilon\sigma_{ST\_B}T_W^4\pi dL - \varepsilon\sigma_{ST\_B}T_0^4\pi dL \tag{18}$$

is the heat sink through the radiation (here, we consider temperature in Kelvin), and

$$W_{conv} = \delta(T_W - T_0)\alpha_{conv}\pi dL \tag{19}$$

is the convection heat sink. Eqs (17-19) are obtained in assumption that thermal conductivity and the radiation coefficient

Here, T_0 is the ambient temperature, $T_{W,MEAN} = ((T_{MAX} + T_0)/2)$ is the wire mean temperature, d and L are the diameter and length of the wire, respectively, S is the wire cross-section, λ is the thermal conductivity of the wire material, σ_{ST_B} is the Stefan–Boltzmann constant, ε is the emissivity of the wire, α_{conv} is the convection heat transfer coefficient, $\delta = 1$ if the wire is placed in atmosphere, and $\delta = 0$ if the wire is placed in vacuum. Equations (17-19) are obtained with the assumption that the thermal conductivity and emissivity do not depend on temperature. This is a reasonable assumption for an order-of-magnitude estimate, because in the temperature range up to several hundred Celsius degrees these parameters are weakly dependent on temperature.

Introducing parameter $\Delta T = (T_{W,MEAN} - T_0)/2$ (denoting overheating of the wire), the following relation between ΔT and W_{beam} can be obtained:

$$\Delta T = \frac{W_{beam}}{8\lambda S / L + 4\varepsilon\sigma_{ST\_B}T_0^3\pi dL + \delta\alpha_{conv}\pi dL}. \tag{20}$$

For parameter α_{conv}, we use the equation for convection of a cylinder by air with speed ν, i.e.,

$$\alpha_{CONV} = 4.13\frac{v^{0.8}}{d^{0.2}}. \tag{21}$$

An important parameter of the VWM is its response time that represents the thermal inertia of the wire and it can be estimated as follows:

$$\tau = \frac{c\rho}{8(\lambda / L^2 + 2\varepsilon\sigma_{ST\_B}T_0^3 / d + \alpha_{conv} / 2d)}, \qquad (22)$$

In case of vacuum, the value of α_{conv} should be set to zero.

Thermal inertia of a wire imposes certain restrictions on the scanning speed of the beam. We have performed dedicated research on the effect of scanning speed on the measurement results of a semiconductor laser beam. Since the profile of such a beam was not known a priori, we took coincidence of scans in forward and backward directions as a criterion for adequacy of measurement results. The measurement results for a stainless steel wire (in air) are shown in Fig. 27 (see [29]).

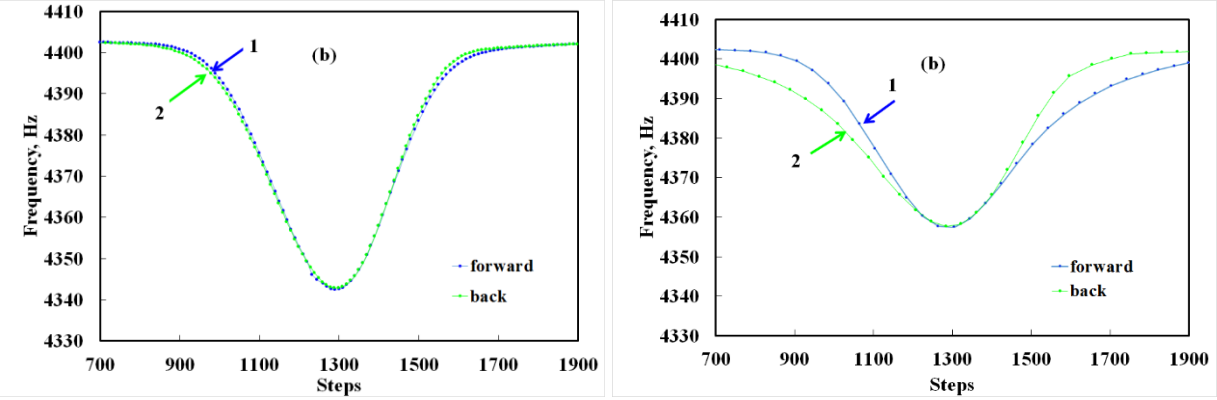

Fig. 27. Forward and backward scans of VWM. Forward (backward) represents movement with increasing (decreasing) number of steps. (a) Scanning with speed of 50 steps/s (0.0830 mm/s). Curves 1 and 2 are forward (movement in the direction of increasing step) and backward scans, respectively. (b) Scanning with speed of 200 steps/s (0.3322 mm/s).

Comparative characteristics of forward and backward scans are presented in Tab. 2

Table 2. Comparative characteristics of forward and backward beam scans at different speeds.

Speed, mm/s	Beam FWHM, mm	Beam FWHM scan time, s	Measurement numbers	Frequency drop, Hz	Coincidence of the scans, Hz	Profile measurement accuracy, %
0.0166	0.556	33.5	987	68	0.11	0.16
0.0332	0.553	16.6	492	63	0.20	0.32
0.0830	0.566	6.8	194	60	0.42	0.70
0.1661	0.602	3.6	97	51	1.03	2.01
0.2491	0.622	2.6	63	50	2.45	4.89
0.3322	0.715	2.1	48	45	3.22	7.15

Note that such preliminary measurements are desirable for other types of wire and measurement conditions (e.g., in vacuum or other atmosphere).

In Table 3, we summarize the thermal parameters of a VWM with a tungsten wire. The VWM can operate in air or in vacuum. In the last column (i.e., total power loss in vacuum), the convection losses are not included.

Table 3. Thermal parameters of VWM with tungsten wire.

Wire temperature rise, K	Frequency, Hz	W_{conv}, W	W_{λ}, W	W_{rad}, W	$W_{total\ in\ air}$, W	$W_{total\ in\ vacuum}$, W
0	6.51×10^{3}	0	0	0	0	0
0.001	6.51×10^{3}	2.14×10^{-7}	2.72×10^{-7}	5.02×10^{-8}	5.36×10^{-7}	3.22×10^{-7}
0.01	6.51×10^{3}	2.14×10^{-6}	2.72×10^{-6}	5.02×10^{-7}	5.36×10^{-6}	3.22×10^{-6}
0.1	6.51×10^{3}	2.14×10^{-5}	2.72×10^{-5}	5.02×10^{-6}	5.36×10^{-5}	3.22×10^{-5}
1	6.51×10^{3}	2.14×10^{-4}	2.72×10^{-4}	5.04×10^{-5}	5.36×10^{-4}	3.22×10^{-4}
10	6.47×10^{3}	2.14×10^{-3}	2.72×10^{-3}	5.28×10^{-4}	5.38×10^{-3}	3.25×10^{-3}
100	6.04×10^{3}	2.14×10^{-2}	2.72×10^{-2}	8.22×10^{-3}	5.68×10^{-2}	3.54×10^{-2}
200	5.52×10^{3}	4.27×10^{-2}	5.43×10^{-2}	2.58×10^{-2}	1.23×10^{-1}	8.01×10^{-2}
400	4.30×10^{3}	8.55×10^{-2}	1.09×10^{-1}	1.11×10^{-1}	3.06×10^{-1}	2.20×10^{-1}
600	2.55×10^{3}	1.28×10^{-1}	1.63×10^{-1}	3.14×10^{-1}	6.05×10^{-1}	4.77×10^{-1}

One can see that the thermal losses by convection and thermal conductivity are in the same order, whereas the losses through the radiation become significant at overheating temperatures higher than 100 K.

In Table 4, we summarize the same thermal parameters as above of a VWM with a stainless steel wire.

Table 4. Thermal parameters of VWM with stainless steel wire.

Wire temperature rise, K	Frequency, Hz	W_{conv}, W	W_{λ}, W	W_{rad}, W	$W_{total\ in\ air}$, W	$W_{total\ in\ vacuum}$, W
0	6.01×10^{3}	0	0	0	0	0
0.001	6.01×10^{3}	2.14×10^{-7}	2.67×10^{-8}	5.02×10^{-8}	2.91×10^{-7}	7.69×10^{-8}
0.01	6.01×10^{3}	2.14×10^{-6}	2.67×10^{-7}	5.02×10^{-7}	2.91×10^{-6}	7.69×10^{-7}
0.1	6.01×10^{3}	2.14×10^{-5}	2.67×10^{-6}	5.02×10^{-6}	2.91×10^{-5}	7.69×10^{-6}
1	5.99×10^{3}	2.14×10^{-4}	2.67×10^{-5}	5.04×10^{-5}	2.91×10^{-4}	7.71×10^{-5}
10	5.78×10^{3}	2.14×10^{-3}	2.67×10^{-4}	5.28×10^{-4}	2.93×10^{-3}	7.95×10^{-4}
100	3.07×10^{3}	2.14×10^{-2}	2.67×10^{-3}	8.22×10^{-3}	3.23×10^{-2}	1.09×10^{-2}

Thermal characteristics of VWM sensors for wires made of different materials are given in Table 5. Here, the wire length is 40 mm and the diameter is 0.1 mm.

Table 5. Thermal characteristics of VWM.

	Frequency resolution, Hz	Thermal resolution, mK	Deposited power resolution (air), mkW	Deposited power resolution (vacuum), mkW	Response time (air), s	Response time (vacuum), s	Dynamic range
Stainless steel	0.01	0.3	0.007	1	20	0.23	7.1×10^{5}
Bronze	0.01	0.6	0.05	2.6	9	0.21	3.5×10^{5}
Tungsten	0.01	1	0.3	5.4	2	0.16	4.4×10^{5}

It should be noted that we fully calculated the sensor response time, considering only the thermal processes occurring in the wire. In autogeneration boards, the feedback circuit uses a capacitor with different values, which affects the start time of the vibration generation. It was interesting to compare the performance of the monitor with two significantly different capacitor values when a heating source per wire is turned on abruptly. Heating was simulated by turning the laser light on/off on the wire.

Recording the corresponding frequency change showed that the time characteristics of the monitor did not change (see Fig. 28).

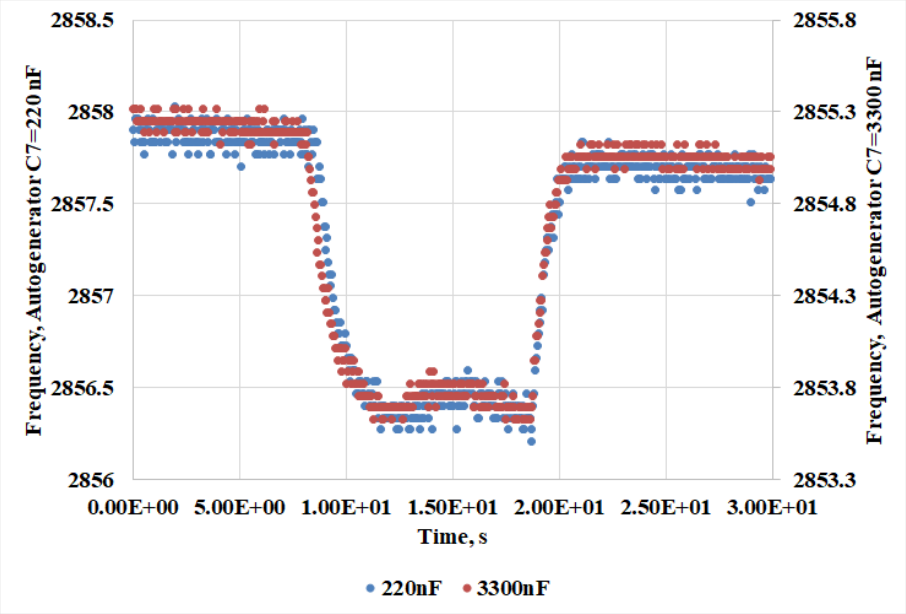

Fig. 28: Response of vibrating wire monitor to abrupt on/off of heating source when using different capacitor C values in autogeneration board. Blue line corresponds to C = 220 nF and brown line to C = 3300 nF.

From the point of view of oscillation amplitude stabilization, C = 3300 nF value is preferable, although it increases the time of the autogeneration mode setting when the monitor power supply is switched on (compare Figs. 7 and 8).

2.3. Beam energy losses in matter

The most important parameter for a given configuration of measured particles and a VWM with a wire of a specific material is the energy that one particle loses when penetrating the wire (parameter W_{beam} in Eq. (20)). The rule of energy loss calculations is strongly dependent on the type of particles.

2.3.1. Protons/ions

For heavy particles (protons and ions), parameter W_{beam} in Eq. (20) is determined by the ionization losses of the particles penetrating the wire material. The equation for specific ionization losses dE/dx of a particle with mass $M >> m_e$ (m_e - electron mass) and velocity v is known as the Bethe–Bloch formula, which is the basic expression used for energy loss calculations [30],

$$-\frac{dE}{dx}=2\pi N_A r_e^2 m_e c^2 \rho \frac{Z}{A}\frac{z^2}{\beta^2}\left[\ln\left(\frac{2m_e c^2\gamma^2\beta^2 W_{\max}}{\Phi^2}\right)-2\beta^2-\delta-2\frac{C}{z}\right], \qquad (23)$$

where $2\pi N_A r_e^2 m_e c^2 = 0.1535\times10^{-4}$ MeV·m^2/mol, $N_A = 6.022\times1023$ mol^{-1} – Avogadro's number, $r_e = 2.817\times10^{-15}$ m is the classical electron radius, ρ is the density of the absorbing material in g/cm^3, Z is the atomic number of the absorbing material, z is the charge of the incident particle in units of

electron charge, A is the atomic weight of the absorbing material in g/mol, Φ is the mean ionization potential in eV, $\beta = v / c$; $\gamma = 1/\sqrt{1-\beta^2}$, c is the speed of light, δ is the amendment that considers the effect of medium density, C is the correction effect of the binding of the electrons on K- and L-shells, and $W_{\max}$ is the maximum energy transfer in a single collision. The maximum energy transfer in the case of proton mass $m_{\mathrm{p}} >> m_{\mathrm{e}}$ is $W_{\max} \approx 2m_e c^2 \gamma^2 \beta^2$. Equation (23) works well for protons and ions. For electrons and positrons, the Bethe−Bloch formula differs from Eq. (23).

In Table 6, some typical values for the proton ionization losses in tungsten (Z = 74, A = 183.84 g/mol, ρ = 19.3 g/cm^3) are presented without corrections in two proton energy ranges.

Table 6. Ionization losses dE_{p} / dx for proton in tungsten (E_{p} is proton kinetic energy).

E_{p}, MeV	dE_{p} / dx, MeV/cm	E_{p}, MeV	dE_{p} / dx, MeV/cm
10	384.63	1000	23.87
11	359.92	2000	22.63
12	338.57	3000	23.04
13	319.92	4000	23.66
14	303.46	5000	24.29
15	288.83	6000	24.88
16	275.73	7000	25.43
17	263.91	8000	25.92
18	253.20	9000	26.37
19	243.44	10000	26.79
20	234.50		
21	226.29		
22	218.71		
23	211.70		
24	205.18		
25	199.11		

For one proton, the energy loss, δ_{p}, in the wire can be approximated as

$$\delta_p = \left(\frac{dE_p}{dx} \right) \times (\pi d / 4). \qquad (24)$$

Some of the proton energy losses will be transferred as heat in the wire material. The ratio of this energy transport, $\varepsilon_{\mathrm{heat}} \approx 0.3$–$0.7$, depends on the proton energy, parameters of the wire material, and wire geometry. Typically for preliminary calculations, we set $\varepsilon_{\mathrm{heat}} \approx 0.3$.

The equation that determines the frequency shift of the wire oscillation depends on the proton beam current I_p, penetrating the wire as follows:

$$\frac{\Delta F}{F_0} = -\frac{E}{2\sigma_0}\frac{\alpha_W \varepsilon_{heat}(\delta_p I_p / e)}{\left[8\lambda S / L + 4\varepsilon\sigma_{ST\text{-}B}T_0^3\pi dL + \eta\alpha_{conv}\pi dL\right]}. \quad (25)$$

2.3.2. Electrons, positrons, muons, photons

Modified Bethe–Bloch formulae for ionization losses for electrons and positrons can be found in[37]. To estimate the electron energy losses in matter, processes besides ionization should also be considered [2]: creation of electron–positron pairs, secondary electron emission (SEM, at low energy), emission of photons, elastic and inelastic scattering, dislocations, production of secondary particles (at high energy), Cherenkov radiation, bremsstrahlung radiation, and optical transition radiation (OTR). The corresponding data for electrons moving in lead are presented in[38].

A unique case is the interaction of muon beams with matter. Muon accelerator is an interesting type of accelerator that offers unique potential for particle physics applications. The concept of a muon collider was first proposed in 1969 [31]. A particular muon accelerator program (MAP) was initiated in 2010, aiming at developing the concepts and technologies required for muon colliders and neutrino factories [32]. An example of muon losses in copper due to various interaction processes can be found in [2].

The loss of photon beams in a material depends on the photon energy and the composition of the material. For energies of the photon (x-ray, gamma ray, bremsstrahlung) from 1 keV to 20 MeV, energy-absorption coefficients for elements Z = 1 to 92 and 48 additional substances of dosimetric interest are presented in[39].

2.4. VWM applications

VWMs are applicable in various configurations for different purposes. Below are the examples of such applications. Section 4.1 presents VWM applications for the accelerator beam diagnostics that have already been tested. Some of the results were reported in detail elsewhere. Section 4.2 presents new applications of the VWM for accelerator diagnostics. Proposals for the use of wires separated by a screen, and for composite wires to measure neutron beams are introduced based on our previous studies. A proposal for the use of the vibrating wire technology for measuring the impact of radiation (including neutrons) on the elastic properties of materials is newly made here. Non-thermal applications of vibrating wires are described in Section 5.

2.4.1. VWMs already implemented for accelerator diagnostics

Electron beam scanners

Initial experiments on scanning charged particle beams were conducted on the electron beam of the synchrotron injector of Yerevan Physics Institute with energy 50 MeV and average current of

[37] I. Wingerter-Seez, Particle physics instrumentation, arXiv:1804.11246v1 physics.ins-det] 30 Apr 2018.
[38] K.A. Olive et al. Passage of particles through matter, Chin. Phys. C, 38, 090001 (2014) and 2015 update.
[39] J.H. Hubbell, S.M. Seltzer, X-Ray Mass Attenuation Coefficients, NIST Standard Reference Database 126, 2004, DOI: https://dx.doi.org/10.18434/T4D01F

approximately 10 nA after collimation [33] (see Fig. 29). A monitor with a large aperture formed by a 50-mm-long target wire was also used to measure the electron beam profile (see [22]).

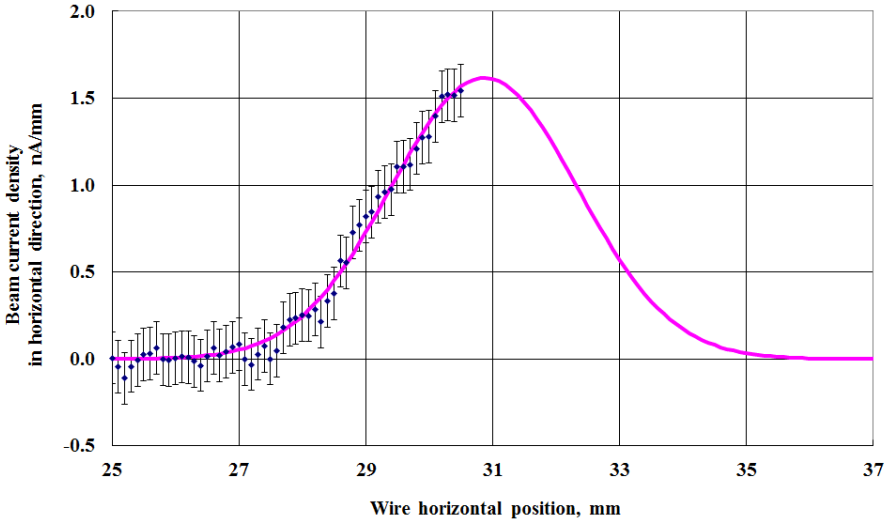

Fig. 29. First experimental results of transverse profile measurements applying vibrating wire scanner on electron beam at Yerevan synchrotron injector. Horizontal profile of 6 nA beam was reconstructed from frequency scan. The beam feed system restricted the scanner movement only to the half of the beam. Nevertheless, this experiment showed for the first time the response of the vibrating wire to a sufficiently small current of the electron beam.

Proton beam scanners

A series of experiments on the use of a VWM on a proton beam was conducted at the PETRA accelerator at DESY, where PETRA serves as a proton booster for HERA. The unique characteristics of the VWM allowed measuring the halo region of the proton beam with an average current of approximately 15 mA and energy of 15 GeV [34, 35] (see Fig. 16 and[40],[41]). From Fig. 30b one can see that frequency response on wire position is started at immediately at movement from parking position (Pos = 0 mm), while the photomultiplier signal begins to form at a much greater depth of scanning (Pos = 14 mm).

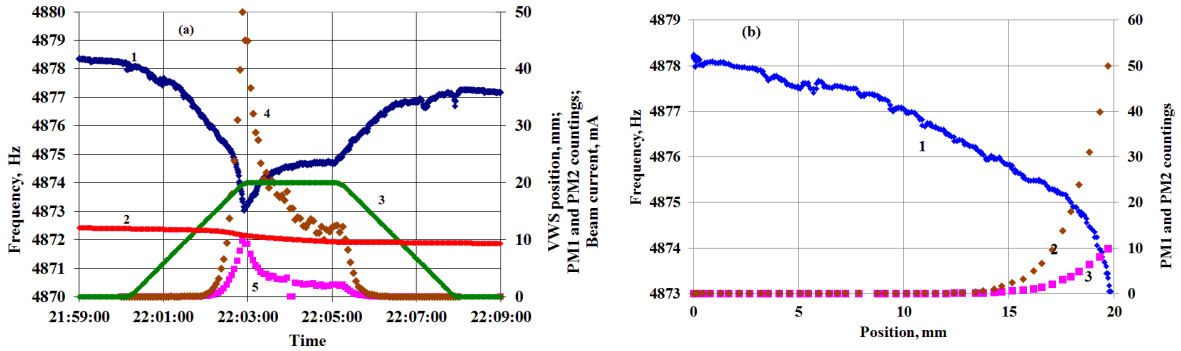

[40] S.G. Arutunian, M. Werner, K. Wittenburg, Beam tail measurements by wire scanners at DESY - ICFA Advanced Beam Dynamic Workshop: Proc. Beam HALO Dynamics, Diagnostics, and Collimation (HALO`03) (in conjunction with 3rd workshop on Beam-beam Interaction), Gurney`s Inn, Montauk, N.Y. USA, May 19-23, 2003

[41] S.G. Arutunian, A.E. Avetisyan, N.M. Dobrovolski, M.R. Mailian, I.E. Vasiniuk, K. Wittenburg, R. Reetz, Problems of Installation of Vibrating Wire Scanners into Accelerator Vacuum Chamber, Proceedings 8th European Particle Accelerators Conference, Paris, France (2002), pp. 1837-1839.

Fig. 30. PETRA (DESY) proton beam scan by VWM: (a) time dependence, 1 - frequency signal, 2 - proton beam current, 3 - scan depth, 4, 5 – responses of photomultipliers, (b) position dependence, 1 - frequency signal, 2, 3 – responses of photomultipliers

A monitor with an expanded aperture of 60 mm and a total wire length of 120 mm was installed on the transport line between the linear accelerator and the 3-GeV synchrotron of the J-PARC complex. The ability of the monitor to diagnose a beam halo was confirmed. As a positive characteristic, it was noted that the sensor was insensitive to secondary electrons[42].

The extended aperture of the VWM was planned to be used to study the proton beam halo in the Project-X Injector Experiment (PXIE, Fermilab), which was an R&D program for developing a multi-megawatt superconducting proton accelerator. The VWM was tested on a Fermilab high-intensity neutrino source (HINS) set-up with a 50-keV proton beam [23, 24].

Proton beam profiling in air by a VWM was conducted at the Korea Multi-purpose Accelerator Complex (KOMAC) facility under low (100 nA) beam-current conditions [36, 20].

Ion beam scanners

A VWM was tested on a beam of iron ions with energy of 20 keV and a current of 16 pA of the EMAL-2 energy-mass analyzer. A frequency shift at a level of 0.15 Hz was obtained (see [35]).

Laser beam scanners

Generally laser beams, as the most accessible heat sources for experiments, are used in the process of developing and calibrating all types of VWMs. Specifically, conventional semiconductor lasers with a power from a few to several hundred mW are used. The laser beam profiling itself, however, may be an independent research topic of interest[43].

X-ray (undulator) radiation scanners

Although X-ray radiation only deposits a small part of its energy in the wire, owing to the high sensitivity of VWMs, this energy is sufficient to heat the vibrating wire at the level of the frequency shift resolution. Experiments were performed at the APS-ANL to measure the X-ray profile from an undulator with an energy range of 6.5–19.5 keV and an unfocused beam of size 3 mm × 1.5 mm. An important task in this experiment was to measure the radiation only from the undulator, with suppression of the background by the softer synchrotron radiation photons generated when the electrons pass the magnetic fields of the focusing and deflecting magnets. This suppression was achieved by a beryllium filter plate. Consequently, only the X-ray emission of the undulator remained after the filter, which was measured by the VWM [25]. Experiments with two vertically-offset horizontal stainless steel wires for temperature diagnostics were conducted at APS beamline 19-ID (flux details: 1×10^{13} X-ray photons/s/mm^2, wavelength range 2.032–0.670 Å, energy range 6.1–18.5 keV, focused beam size 83 μm × 38 μm, and unfocused beam size 2.4 mm × 1.2 mm[44])

[42] K. Okabe, M. Yoshimoto, K. Yamamoto and M. Kinsho, A preliminary study of the vibration wire monitor for beam halo diagnostic in J-PARC L3BT, Proceedings International Particle Accelerator Conference IPAC2013, Shanghai, China (2013), pp. 535-537.
[43] M.A. Aginian, S.G. Arutunian, V.A. Hovhannisyan, M.R. Mailian, K. Wittenburg, Vibrating wire scanner/monitor for photon beams with wide range of spectrum and intensity.- NATO Advanced Research Workshop "Advanced Photon Sources and Their Application" Nor Amberd, Armenia, August 29 - September 02, 2004
[44] See in https://www.aps.anl.gov/Beamlines/Directory/Details?beamline_id=27

Owing to the high sensitivity of this technique, the studies were performed at extremely low power levels using the radiation from a 3.3-cm-period permanent magnet hybrid undulator with a 5-mA electron beam at an energy of 7 GeV. The X-ray beam was filtered by transmission through 7 mm of beryllium placed in the photon beam path, ensuring that only hard X-rays were detected. The VWM was installed in the vacuum chamber of the beamline with the vacuum level decreased to 10^{-9} Torr[45]. Results of the undulator X-ray beam measurements are presented in Fig. 31.

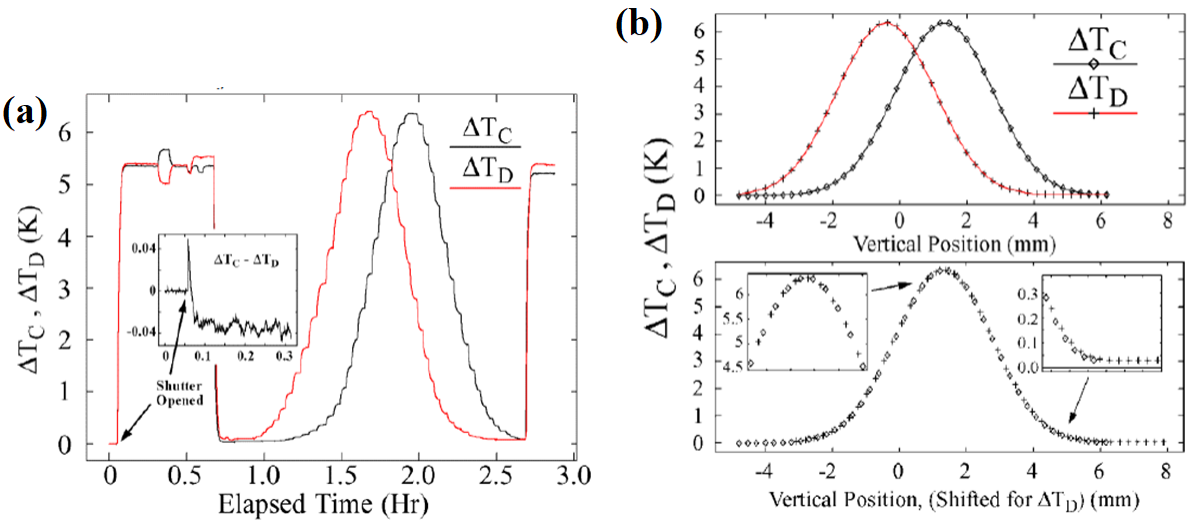

Fig. 31. Undulator X-ray beam measurement by two-wire VWM at APS-ANL. (a) Data collected during vertical angle scan. (b) VWM data corrected for thermal drift and beam current decay. Two data sets are overlapped by introducing some offset in lower panel for direct comparison [25].

Synchrotron radiation scanners

At the APS-ANL synchrotron, an experiment was conducted to measure the parameters of the electron beam using the synchrotron radiation (SR). It is important that such a measurement is conducted outside the vacuum chamber behind the copper flange of one of the unused SR channels. In general, radiation with a power of approximately 99.1 W and a peak energy of approximately 10 keV was absorbed by a 6-mm-thick copper flange, and only hard X-ray photons with an energy of more than 100 keV (SR spectrum tail) with a power of 420 mW passed through the flange. Approximately 1.1 mW of the power was converted into heat and deposited on the wire. The electron beam of the synchrotron, using the magnetic optics of the accelerator, was scanned in an angle within the limits of 300 μrad with a step of 2.4 μrad. A special five-wire monitor was developed. Profile of the synchrotron radiation was obtained in the vertical direction in air [26]. A picture of the VWM and the profiling results are presented in Fig. 32.

[45] Advanced photon source safety assessment document, Argonne National Laboratory, APS-3.1.2.1.0, Rev. 5, (APS_1188832).

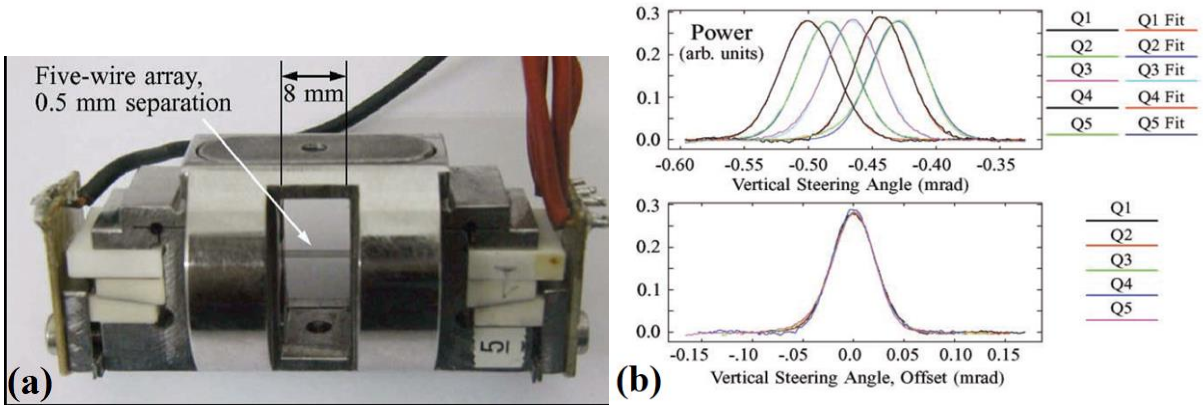

Fig. 32. Synchrotron radiation vertical profile measurements by five-wire VWM at APS-ANL. (a) Monitor details. (b) APS bending magnet radiation power density profiles inferred from the VWM data. Top: Measured profiles together with Gaussian fits. Bottom: The same measured data, shifted along the horizontal axis.

In[46], the mutual thermal influence of the wires on each other was considered and included when determining the profile.

Large-aperture monitors

Monitors with a large aperture size are of interest for profiling large proton beams (up to 80 mm). Two types of such monitors are developed:

• Direct action of the beam on a vibrating wire: a distinct scheme of the shock excitation of the process of autogeneration of oscillations is added to the electronic circuit [22, 37].

• Yoke type with two mechanically connected wires: a non-vibrating target wire of increased length that is exposed by the beam, and a vibrating wire measuring the change in the tension of the target wire are used together.

A yoke-type VWM with the length of the target wire, 60 mm, is presented in Fig. 33. Measurement of the temperature/tension of the target wire was performed using a special link between the two wires. The aperture of such monitors can reach 80 mm [23, 24]. The obtained data, including the beam test results at the HINS facility, indicate that the large-aperture VWM could be a useful diagnostic instrument in numerous present and future accelerators and be particularly effective for transverse beam halo measurements.

[46] S.G. Arutunian, G. Decker, G.S. Harutyunyan, I.E. Vasiniuk, Heat coupling in multi-wire vibrating wire monitor, Proceedings 21st Russian Particle Accelerators Conference, Zvenigorod, Russia (2008), pp. 247-249.

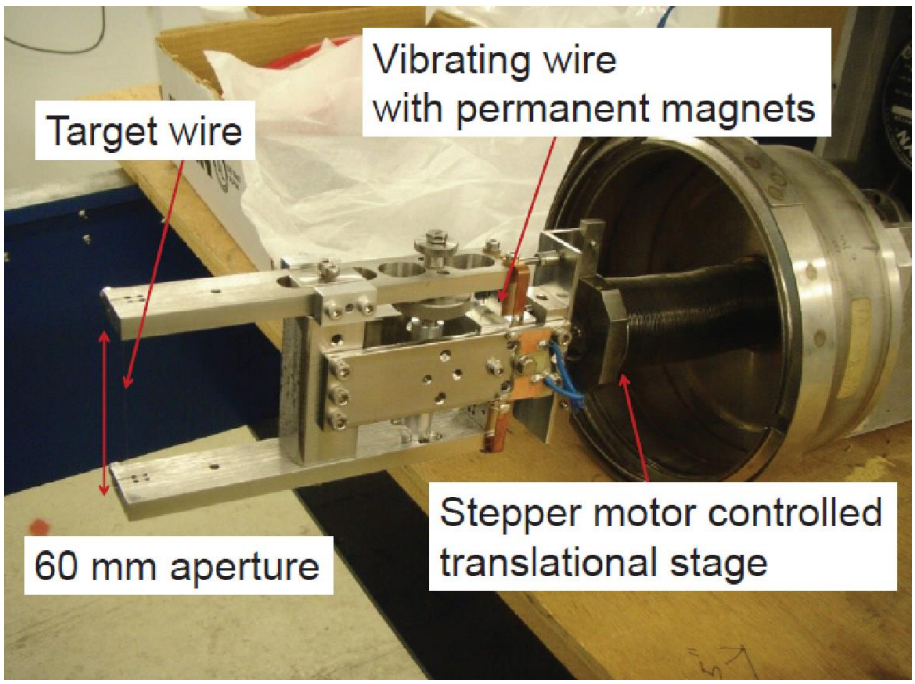

Fig. 33. Large-aperture yoke-type vibrating wire monitor assembly. Two mechanically connected wires: target wire of 60 mm length exposed to the beam and a vibrating wire for sensing the tension of the target wire.

2.4.2. New proposals for VWM applications based on thermal method

Double-wire beam position monitors

Monitors with two wires spaced a few millimeters apart allow a differential method to control the beam shift between the wires. The method of differentiation of the signals of two wires can also be used to normalize monitors considering the influence of ambient temperature and the presence of other backgrounds besides the direct impact of the measured beam (one of the two wires is exposed to the beam, whereas the other wire is protected from the beam by a special screen and provides a reference signal). In[47], a type of double-wire monitor with an aperture increased by 8 mm is presented. This modification has a shorter response time and can be used both in vacuum and air.

A novel double-wire vibrating wire monitor (DW-VWM) consists of two wires spaced by a screen. Such a monitor is being developed for high-intensity accelerators, such as the joint European–Japanese project, IFMIF, specifically for the linear IFMIF prototype accelerator (LIPAc) (for details see[48]). The specific feature here is the high accelerator current (approximately 125 mA of the average beam current), which dictates the need for precise measurement of the flux of the lost particles and the halo region of the beam.

VWM with multilayer (composite) wires

A proposal on unique type of VWM with wires covered by a gadolinium layer was made for thermal neutron beam profiling [18]. Two unique properties are combined here: the unprecedented sensitivity

[47] M. Chung, S.G. Arutunian, G.S. Harutyunyan, D. Kwak, E.G. Lazareva, A.V. Margaryan, M.A. Tumanyan, Double-wire vibrating wire monitor (dw-vwm) for beam halo monitoring in high-intensity accelerators, Proceedings of 8th International Beam Instrumentation Conference, IBIC2019, Malmo, Sweden (2019), pp. 373-376.
[48] Overview of the IFMIF/EVEDA project, URL: https://iopscience.iop.org/article/10.1088/1741-4326/aa6a6a/pdf

of the natural frequency of a clamped vibrating wire to the wire temperature, and the remarkable ability of some gadolinium isotopes for neutron capture. ^{157}Gd has the highest thermal neutron capture cross-section among all the stable isotopes in the periodic table. We propose to measure the temperature increase in the wire containing gadolinium isotopes, which occurs when neutrons penetrate the wire and deposit some energy into the wire. We developed two types of VWMs for neutrons: small-scale with an approximately 10-μm-diameter tungsten wire and approximately 2-μm-thick Gd layer, and middle-scale with approximately 100-μm-diameter tungsten wire and an approximately 10-μm-thick Gd layer. For the first type, we offer to employ ^{157}Gd, which allows capturing all the thermal neutrons falling on the wire. For the second type, it is possible to use natural Gd.

VWM for elastic properties investigation

VMWs can also be useful for studying the effects of neutron fluxes on the elastic properties of the vibrating wire material. It is known that neutron fluxes when passing through a substance can affect its parameters, in particular, the mechanical properties of metals. The change in the mechanical properties of metals is caused by both neutron capture (mainly for neutrons with energy less than 1 MeV) and lattice disturbance during the atom-neutron collisions with energy more than 1 MeV. One of the mechanical parameters subject to changes under neutron irradiation is the elastic property of metals. In particular, there is noteworthy embrittlement of the materials, which reduces the lifetimes of the structures and assemblies in which these materials are used. It is proposed to use a vibrating wire exposed in the neutron flux, to observe the effect of neutron irradiation impact on the elastic properties of metals. The change in the elastic properties of the wire will be reflected in the values of the natural oscillation frequency of the wire and recorded accordingly. To determine the effect of the influence of a neutron flux on the oscillation frequency of the wire, it is proposed to use overstressed resonators, in which the wire is stretched by a tension comparable to the tensile limit of the materials (we typically used resonators in which the wire tension was less than this limit). It is suggested that a differential measurement scheme be used to compensate thermal and creep-related drifts of an overstressed material. A two-wire monitor, in which two wires are located in the same thermal space and are separated by a screen that significantly differentiates the exposure of neutrons to the wires, appears adequate to the task. The proposed method will allow characterizing the effects of neutron fluxes by comparison of the changes in the frequencies of both the wires.

2.5. Other methods of using vibrating wire sensors

The proposals below concern the use of vibrating wires as a resonant target as well as for measuring thin beams. These proposals may be of great interest for accelerator diagnostics, however, at the moment they have been tested only on semiconductor laser beams and these preliminary results have been reported elsewhere (see Refs. [27, 38, 39, 40, 41]).

2.5.1. Vibrating wire as resonance target

Recently, a new type of wire scanner for beam profile measurements was developed based on the use of a vibrating wire as a scattering target. Synchronous measurements with wire oscillations allow detecting only the signal originating from the scattering of the beam on the wire. This resonant method enables fast beam profiling in the presence of a high level of background. The concept was suggested in [38], and for photon beams it was realized in [39]. The method can be applied to different types of

beams by simply choosing an appropriate detector for each case. For photon beams, fast photodiodes can be used, and for charged particles, scintillators combined with photomultipliers etc. are used.

The results of laser beam scans in a dedicated arrangement of laser and photodiode positions in which the photodiode registers two very similar peaks of different origins (one is caused by reflections from the vibrating wire and the other from the holder of the monitor) are presented in Fig. 34.

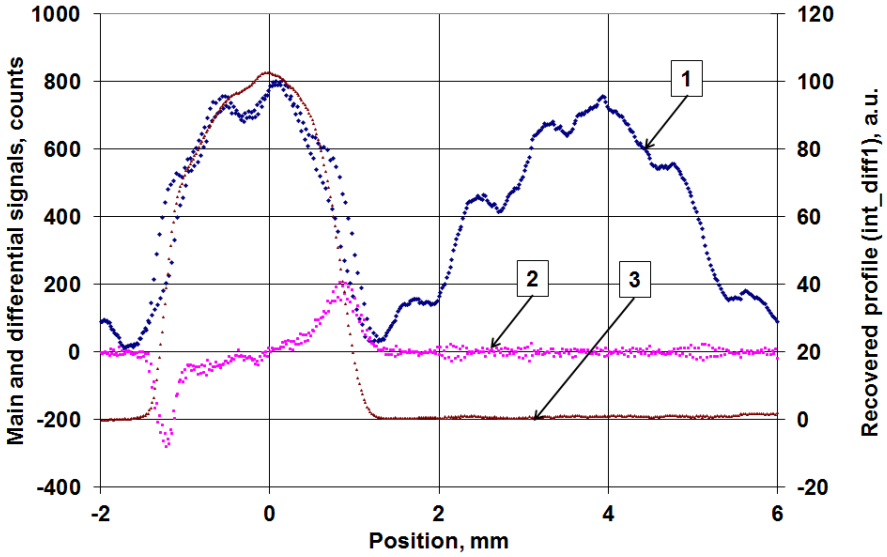

Fig. 34. Vibrating wire as resonance target: photodiode measures reflections from both the vibrating wire and other mechanical parts of the resonant-type vibrating wire sensor (1, blue curve). Only the first type of the photodiode signal contributes to the differential signal (2, magenta curve). The algorithm developed in this study recovers the laser beam profile (3, brown curve).

In this experiment, the speed of the scanning does not exceed the speed of the wire during oscillations; however, even in this case, the time of full scanning can be reduced to approximately 100 ms. In [40], it is theoretically proved that the method can be applied using comparatively much higher scanning speeds. The increase in the scanning speed allows the method to be applied for the tomography of beams, i.e., for restoring a 2D profile of a beam by a set of one-dimensional scans performed at different angles in the transverse plane of the beam. The first attempt to use a VWM for laser beam tomography was tested in [41].

2.5.2. Vibration wire as miniature scanner for thin beam profiling

The measurement of beams of micrometer sizes is an important task in accelerator physics. A method for the profile measurements of small transverse size beams using a vibrating wire was proposed in [27, 39]. The main concept is to use the vibrating wire motion during its oscillations as the scanning mechanism and to synchronously measure the scattered/reflected particles/photons created by the interactions of the measured beam with the wire. The method is expected to be applicable to thin beams in particle accelerators. First, experimental results of a focused laser beam scanning were obtained in [27]. The concept was based on the measurement of reflected photons of a laser beam from the wire. The proof-of-principle test results, obtained using a laser beam including data processing and absolute calibration of the beam profile, as well as evaluation of the signal to noise ratio of the method, are presented in [28]. The schematic of the beam and vibrating wire interaction as well as obtained profile of the laser are presented in Fig. 35. Positioning of vibrating wire in both the precisely

measured locations allows calibrating the profile in absolute coordinates. Further research will continue in this direction.

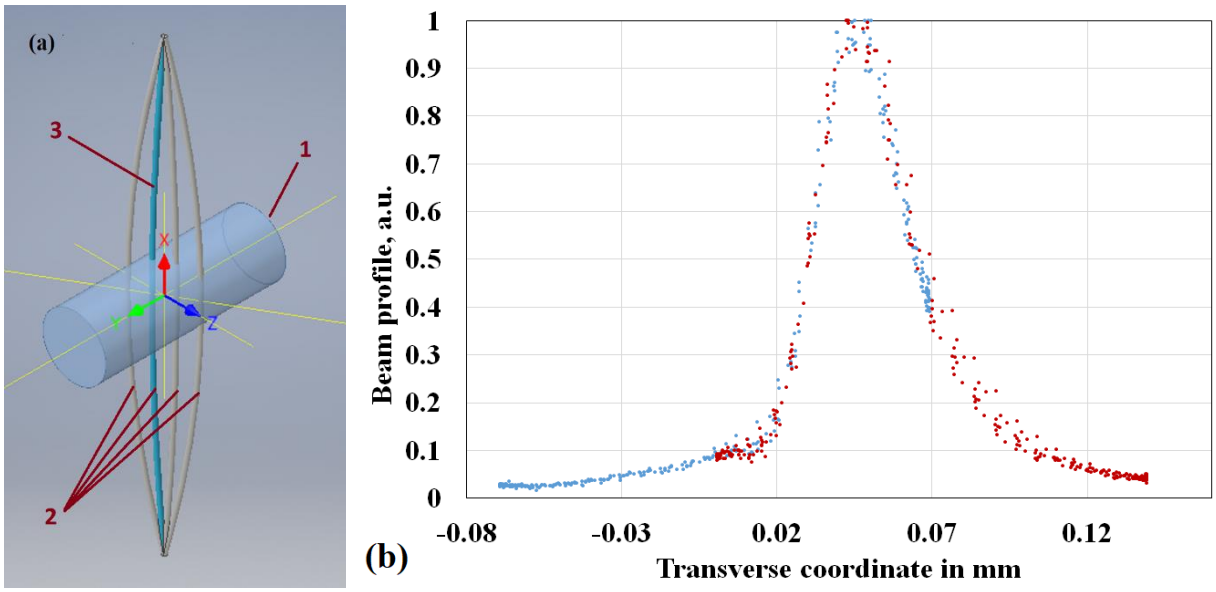

Fig. 35. Schematic of beam and vibrating wire interaction and obtained profile. (a) Beam 1 is intercepted by an oscillating wire. X-axis is directed along the wire at its central position, y-axis is directed along the beam propagation, and z-axis is directed along the beam transverse direction. The positions of the wire at different times during its oscillation are denoted by 2 and 3. (b) Profile of the laser beam in absolute units (mm). Profile is recovered by measurements when the VWM in two positions shifts by 0.07 mm, which allows us to reconstruct the profile in absolute coordinates. Blue dots—profile recovered from measurement at the VWM position of 0.04 mm, orange dots—profile recovered from measurement at the VWM position of 0.11 mm. In [42] upgrade of vibrating wire resonator and measurement system was done. Scanning of the profile in several positions of the vibrating wire monitor allowed us to restore the profile of the beam in absolute coordinates. The method of determining the laser beam profile by superimposing the overlapping profiles in several resonator positions of the vibrating wire is similar to the creation of a panoramic image by stitching procedure. Image stitching is the process that combines images with overlapped areas to form an image with wide view. Usually, after inputting a series of images with overlapped areas, feature matching is applied to find the corresponding points of the images for stitching and then translation is done to align them properly[49]. It is important that this procedure allows to separate the structure inherent to the profile (an analogue of panorama) from that associated with the uncertainty of the wire movements (similar to camera defect).

Reconstruction of the laser beam profile using this procedure is shown in Fig. 36 (see also[50])

[49] Wang Z., Yang Z., Review on image-stitching techniques, Multimedia Systems, Springer, 20 March 2020; https://doi.org/10.1007/s00530-020-00651-y.
[50] Meeri Kim, Vibrating wire scanner to profile micron-sized beams, Scilight, 3 March, 2021.

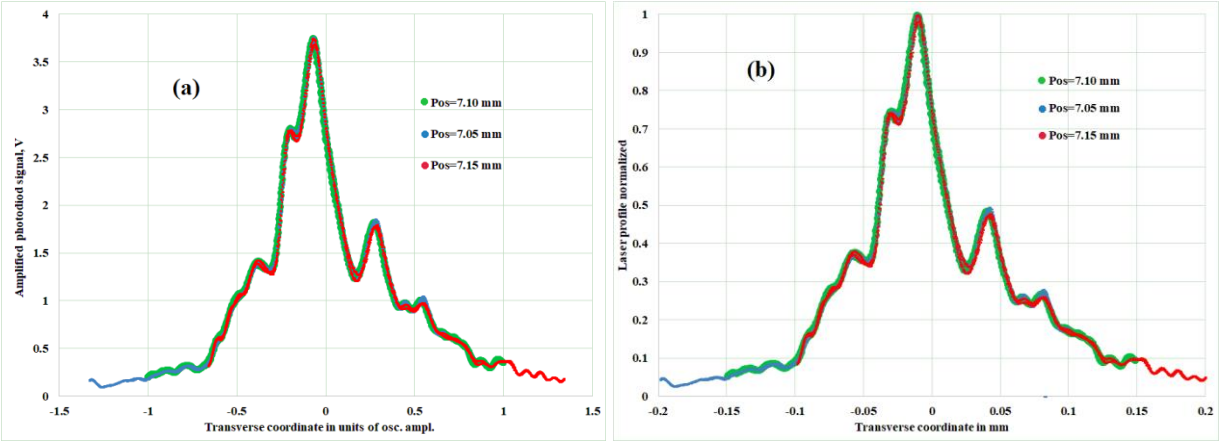

Fig. 36. The reconstruction of the laser beam profile using the numerical differentiation of the primary photodiode signal for n_0 = 3. (a) The transverse coordinate is represented in units of amplitude of the wire oscillations relative to the oscillations center at: 7.10 mm (green), 7.05 mm(blue), and 7.15 mm (red). The transverse shift (in amplitude units of the wire oscillation amplitude) has been appliedto ensure the best matching with the 7.10 mm profile (in areas where these profiles overlap). (b) Reconstructing the laser beam profile in absolute coordinates: resonator position 7.10 mm (green), 7.05 mm (blue), and 7.15 mm (red).

3. Conclusion

The thermal principle of VWMs enables measuring any type of beam that deposits a fraction of its energy in the wire. A wide dynamic range (in the temperature equivalent to fractions of milli Kelvin to hundreds of degrees), high accuracy of the measurements, good long-term stability, resistance to high background radiation and electromagnetic interference, and digital nature of the measurement of the output value (i.e., the frequency of natural oscillations of the wires) make this method a versatile tool for measuring the profiles of beams of charged particles, electromagnetic radiation, and neutrons in a wide range of energies. The large dynamic range, in particular, allows for measurements in both the halo and core of the beam.

It appears that the proposal to use a vibrating wire as the resonance target may also be of interest to accelerator diagnostics, as it allows detecting a well-defined frequency signal from the vibrating wire against the background of numerous particles and electromagnetic radiation unrelated to the beam scattering on the wire.

The proposal to use the motion of the oscillating wire as a scanner opens the opportunity for fast measurement of the profile of thin beams. With further improvement, this method can be developed to a tomographic method for the reconstruction of the two-dimensional profile of a beam. The method is promising both for accelerator diagnostics and for wider use of micron-sized beams.

4. Practical work items of students:

- Familiarization with VWM operation principle of vibrating wire sensors/monitors.
- Choice of wire tension corresponding to the given VWM parameters.
- Check proper generation by oscilloscope.
- Wiring of VWM test bench.
- Run the application program (digital oscilloscope) of wire frequency measurement.
- Prepare laser beam profile measurement by means of VWM.
- Measurement the VWM frequency signal at forward and backward scan using the application program.
- Familiarization with electron beam profile measurement by means of VWM.
- Check the communication lines between accelerator area and control room.
- Acquire the data from scan station equipped with VWM by corresponding application program.
- Compare results with beam profile measurement by of YAG:Ce crystal station for AREAL beam profile measurement (see[51])

We hope that the proposed course will help students to quickly master the attainments of beam profiling using vibrating wire monitors, and based on the obtained skills get ready for using other existing methods in their further work.

A detailed description of the practical work done by students is given in a separate manual[52].

5. References

[1] P. Forck, Lecture Notes on Beam Instrumentation and Diagnostics, Gesellschaft fur Schwerionenforschung (GSI) Darmstadt, Germany,Joint University Accelerator School, January – March 2011, pp. 143. URL: https://www-bd.gsi.de/conf/juas/juas_script.pdf.

[2] E. Bravin. Transverse Beam Profiles - 2008. in Proc. CERN Accelerator School on Beam Diagnostics (CAS'08), Dourdan, France, pp. 377-406.

[3] K. Wittenburg, Specific instrumentation and diagnostics for high -intensity hadron beams, DESY, Hamburg, Germany, arXiv:1303.6767 [physics.acc-ph], 2013.

[4] P. Strehl, Beam Instrumentation and Diagnostics, Springer-Verlag, Berlin, Heidelberg, 2006.

[5] D. Brandt, CAS CERN Accelerator School Beam Diagnostics, Dourdan, France, 17 August 2009, p. 597.

[6] H. Koziol, Beam diagnostics for accelerators, CERN, Geneva, Swizterland, URL: http://www.isa.au.dk/accfys/E08/Download/Koziol_BeamDiagnostics.pdf.

[7] G. Kube, Particle beam diagnostics and control, URL: https://bib-pubdb1.desy.de/record/91024/files/KubeLecture.pdf.

[51] Joint German–Armenian Student Practical Course on Accelerator Physics, Armen Grigoryan, Artsrun Sargsyan, Gevorg Zanyan, Vahe Sahakyan, Gayane Amatuni, PracticalCourses_BeamDiagnostics.docx, CANDLE, 2019.
[52] Hands-on lab steps of practical course: Vibrating wire monitors and beam profile measurements.

[8] K. Wittenburg, Beam size measurements using Wire Scanners at Synchrotron Light Sources and FELs or Wire scanners for Electron Beams (excluding Hadron Beams), URL: http://bib-pubdb1.desy.de/record/403403/files/Wire%20Scanner%20Presentation.pdf.

[9] S. Burger, C. Carli, M. Ludwig, K Priestnall, U. Raich, The ps booster fast wire scanner, Proc. Diagn. Instrum Part Acc. Conf. DIPAC03, Mainz, 2003, p. 122-124.

[10] P. Dirksen, M. Lenckowski, W.R. Rawnsley, M. Rowe, V. Verzilov, A Fast Wire Scanner for the TRIUMF Electron Linac, 6th International Beam Instrumentation Conference, IBIC2017, Grand Rapids, 2017, pp.401-403.

[11] M. Veronese, S. Grulja, G. Penco, M. Ferianis, S. Dal Zilio, S. Greco1, M. Lazzarino, L. Fröhlich, A nanofabricated wirescanner: design, fabrication and experimental results, 6th International Beam Instrumentation Conference, IBIC2017, Grand Rapids, MI, USA, 2017, pp. 314-317.

[12] S. Borrelli, M. Bednarzik, C. David, E. Ferrari, A. Gobbo, V. A. Guzenko, N. Hiller, R. Ischebeck, http://accelconf.web.cern.ch/AccelConf/ibic2017/talks/we2ab2_talk.pdf

[13] G. F. Knoll, Radiation Detection and Measurement, John Willey, New York (1999).

[14] E.J. Jaeschke, S. Khan, J.R. Schneider, J.B. Hastings, Synchrotron Light Sources and Free-Electron Lasers, Accelerator Physics, Instrumentation and Science Applications, Springer International Publishing Switzerland 2016.

[15] S.G. Arutunian, A.V. Margaryan, G.S. Harutyunyan, E.G. Lazareva, M. Chung, D. Kwak, D.S. Gyulamiryan, Vibrating wire monitor: Versatile instrumentation for particle and photon beam measurements with wide dynamic range, Journal of Instrumentation, 2021, 16, R01001, 1-33.

[16] S.G. Arutunian, N.M.Dobrovolski, M.R. Mailian, I.G. Sinenko, and I.E. Vasiniuk, Vibrating wire for beam profile scanning, Phys. Rev. Special Topics - Accelerators and Beams, 1999, v. 2, 122801.

[17] S.G. Arutunian, Vibrating wire sensors for beam instrumentation, Beam Instrumentation Workshop, BIW08, (May 4-8, 2008, Lake Tahoe, USA), pp. 1-7.

[18] S.G. Arutunian, J.Bergoz, M.Chung, G.S.Harutyunyan, E.G.Lazareva, Thermal neutron flux monitors based on vibrating wire, NIM A, 797, 37-43 (2015).

[19] F. Bourquin, M. Joly, A magnet-based vibrating wire sensor: design and simulation, Smart Mater. Struct. 14 (2005) 247–256.

[20] M.A. Aginian, S.G. Arutunian, D. Choe, M. Chung, G.S. Harutyunyan, S.-Y. Kim, E.G. Lazareva, A.V. Margaryan, Precise out-vacuum proton beam monitoring system based on vibrating wire, Journal of Contemporary Physics (Armenian Academy of Sciences), 2017, Volume 52, Issue 2, pp 110–120

[21] A.A.H. Padua, J.M.N.A. Fareleira, J.C.G. Calado, W.A. Wakeham, Electromechanical model for vibrating-wire instruments, Rev. Sci. Instrum., 69, 1998, 2392-2399.

[22] A.E. Avetisyan, S.G. Arutunian, I.E. Vasiniuk, M.M. Davtyan, Yerevan Synchrotron Injector Electron Beam Transversal Scan with Vibrating Wire Scanner, Journal of Contemporary Physics (Armenian Academy of Sciences), 46, 6, pp. 247–253, (2011).

[23] S.G. Arutunian, A.E. Avetisyan, M.M. Davtyan, G.S. Harutyunyan, I.E. Vasiniuk, M. Chung, V. Scarpine, Large aperture vibrating wire monitor with two mechanically coupled wires for beam halo measurements, Physical review special topics [

[24] M. Chung, V. Scarpine, B. Hanna, J. Steimel, V. Shiltsev, S.G. Arutunian, S. Artinian, Transverse beam halo measurements at high intensity neutrino source (hins) using vibrating wire method, Proceedings International Particle Accelerator Conference IPAC2013, Shanghai, China (2013), pp. 819-821.

[25] G. Decker, S. Arutunian, M. Mailian, G. Rosenbaum, First vibrating wire monitor measurements of a hard x-ray undulator beam at the Advanced Photon Source, Proceedings European workshop on beam diagnostics and instrumentation for particle accelerators, DIPAC2007, Venice, Italy (2007), pp.36-38.

[26] G. Decker, S. Arutunian, M. Mailian, I. Vasiniuk, Hard X-ray synchrotron measurements at the APS with vibrating wire monitor, Proceedings Beam Instrumentation Workshop, BIW08, Lake Tahoe, USA (2008), pp. 36-40.

[27] E.G. Lazareva, Vibrating Wire for Profile Measurements of Thin Beams in Particle Accelerators: Preliminary Tests Using a Laser Beam, Journal of Contemporary Physics (Armenian Academy of Sciences), 2018, Vol. 53, No. 2, pp. 136–145.

[28] S.G. Arutunian, S.A. Badalyan, M. Chung, E.G. Lazareva, A.V. Margaryan, G.S. Harutyunyan, A method for profile measurements of small transverse size beams by means of a vibrating wire, Rev. Scientific Instruments, 90, 073302 (2019);

[29] S.G. Arutunian, G.S. Harutynyan, D. Choe, M. Chung, E.G. Lazareva, A.V. Margaryan, Effects of Scanning Speed on the Laser Beam Profile Measurements by Vibrating Wire, Journal of Contemporary Physics (Armenian Academy of Sciences), 52, 4, 366–374 (2017).

[30] W.R. Leo. Techniques for Nuclear and Particle Physics Experiments. New York, Berlin, Heidelberg, Springer-Verlag, 1987.

[31] G. Budker, Proceedings 7th International Conference High-Energy Accelelerators, Yerevan, 1970, p. 33. Yerevan: Publ. House Acad. Sci. Armen. SSR (1970).

[32] M.A. Palmer, S. Brice, A.D. Bross, D. Denisov, E. Eichten, R. Lipton, D.V.Neuffer, H. Kirk, R. Palmer, M. Kaplan, P. Snopok, A. Bogacz, C. Ankenbrandt, J-P. Delahaye, P. Huber, Muon accelerators for the next generation of high energy physics experiments, Proceedings International Particle Accelerator Conference IPAC2013, Shanghai, China (2013), pp. 1475-1477.

[33] S.G. Arutunian, N.M. Dobrovolski, M.R. Mailian, I.E. Vasiniuk, Vibrating wire scanner: first experimental results on the injector beam of Yerevan synchrotron. - Phys. Rev. Special Topics, Accelerators and Beams, 2003, v. 6, p. 042801.

[34] S.G. Arutunian, M.R. Mailian, Kay Wittenburg, Vibrating wires for beam diagnostics, Nucl. Instrum. Methods A, 572, 2007, pp 1022-1032.

[35] S.G. Arutunian, K.G. Bakshetyan, N.M. Dobrovolski, M.R. Mayilyan, V.A. Oganessian, A.E. Soghoyan, I.E. Vasiniuk, K. Wittenburg, Vibrating wire scanner parameters optimization, Proceedings 9th European Particle Accelerators Conference, Lucerne, Switzerland (2004), pp. 2457-2459

[36] D. Choe, M. Chung, S.Y. Kim, S.G. Arutunian, A.V. Margaryan, E.G. Lazareva, Beam Halo Measurements using Vibrating Wire at the KOMAC, Proceedings International Particle Accelerator Conference, IPAC2016, Busan, Korea (2016), pp. 680-682

[37] S.G. Arutunian, M.A. Davtyan, I.E. Vasiniuk, Large aperture electron beam scan with Vibrating Wire Monitor in air, Proceedings International Particle Accelerator Conference IPAC2010, Kyoto, Japan (2010), pp. 876-878.

[38] S.G. Arutunian, A.V. Margaryan, Oscillating wire as a “Resonant Target” for beam, Proceedings International Particle Accelerator Conference IPAC2014, Dresden, Germany (2014), pp. 3412-3414.

[39] S.G. Arutunian, M. Chung, G.S. Harutyunyan, A.V. Margaryan, E.G. Lazareva, L.M. Lazarev, L.A. Shahinyan, Fast resonant target vibrating wire scanner for photon beam, Rev. Scientific Instruments, 87, 023108 (2016).

[40] M.A. Aginian, G.S. Harutyunyan, S.G. Arutunian, S.A. Badalyan, M. Chung, E.G. Lazareva, A.V. Margaryan, M.A. Tumanyan, Development of New Algorithm in the Method of a Resonant Vibrating Target for Large Scanning Speeds, Journal of Contemporary Physics (Armenian Academy of Sciences), 2019, Vol. 54, No. 3, pp. 232–241.

[41] M.A. Aginian, J Alonso, S.G.Arutunian, M. Chung, A.V. Margaryan, E.G. Lazareva, L.M. Lazarev, L.A. Shahinyan, New method in medical tomography based on vibrating wire: bench-test experiment on laser beam, IOP Journal of Physics: Conf. Series 826 (2017) 012016, pp. 1-11 (25th Annual International Laser Physics Workshop), doi:10.1088/1742-6596/755/1/011001.

[42] S. G. Arutunian, A. V. Margaryan, G. S. Harutyunyan, E. G. Lazareva, A. T. Darpasyan, D. S. Gyulamiryan, M. Chung, and D. Kwak, Characterization of micrometer-size laser beam using a vibrating wire as a miniature, scanner, Rev. Sci. Instrum. 92, 033303 (2021); https://doi.org/10.1063/5.0028666